Materials Today Bio 26 (2024) 101036

Contents lists available at ScienceDirect

Materials Today Bio

journal homepage: www.journals.elsevier.com/materials-today-bio

TPG-functionalized PLGA/PCL nanofiber membrane facilitates periodontal tissue regeneration by modulating macrophages polarization via suppressing PI3K/AKT and NF-κB signaling pathways

Xiang Han [a,b,c,1], Feiyang Wang [a,b,c,1], Yuzhuo Ma [a,b,c], Xuerong Lv [a,b,c], Kewei Zhang [a,b,c], Yue Wang [a,b,c], Ke Yan [a,b,c], Youmin Mei [d], Xiaoqian Wang [a,b,c,*]

[a] Department of Periodontology, The Affiliated Stomatological Hospital of Nanjing Medical University, Nanjing, 210029, People's Republic of China
[b] Jiangsu Province Key Laboratory of Oral Diseases, Nanjing, 210029, People's Republic of China
[c] Jiangsu Province Engineering Research Center of Stomatological Translational Medicine, Nanjing, 210029, People's Republic of China
[d] Department of Periodontology, Nantong Stomatological Hospital, Affiliated Nantong Stomatological Hospital of Nantong University, Nantong, 226000, People's Republic of China

ARTICLE INFO

Keywords:
Periodontal tissue regeneration
TPG
Electrospinning
Macrophages
Immune microenvironment

ABSTRACT

Traditional fibrous membranes employed in guided tissue regeneration (GTR) in the treatment of periodontitis have limitations of bioactive and immunomodulatory properties. We fabricated a novel nTPG/PLGA/PCL fibrous membrane by electrospinning which exhibit excellent hydrophilicity, mechanical properties and biocompatibility. In addition, we investigated its regulatory effect on polarization of macrophages and facilitating the regeneration of periodontal tissue both in vivo and in vitro. These findings showed the 0.5%TPG/PLGA/PCL may inhibit the polarization of RAW 264.7 into M1 phenotype by suppressing the PI3K/AKT and NF-κB signaling pathways. Furthermore, it directly up-regulated the expression of cementoblastic differentiation markers (CEMP-1 and CAP) in periodontal ligament stem cells (hPDLSCs), and indirectly up-regulated the expression of cementoblastic (CEMP-1 and CAP) and osteoblastic (ALP, RUNX2, COL-1, and OCN) differentiation markers by inhibiting the polarization of M1 macrophage. Upon implantation into a periodontal bone defect rats model, histological assessment revealed that the 0.5%TPG/PLGA/PCL membrane could regenerate oriented collagen fibers and structurally intact epithelium. Micro-CT (BV/TV) and the expression of immunohistochemical markers (OCN, RUNX-2, COL-1, and BMP-2) ultimately exhibited satisfactory regeneration of alveolar bone, periodontal ligament. Overall, 0.5%TPG/PLGA/PCL did not only directly promote osteogenic effects on hPDLSCs, but also indirectly facilitated cementoblastic and osteogenic differentiation through its immunomodulatory effects on macrophages. These findings provide a novel perspective for the development of materials for periodontal tissue regeneration.

1. Background

Periodontitis is a prevalent chronic inflammatory disease characterized by the devastation and absorption of periodontal tissue [1,2]. Gingival inflammation, the development of periodontal pockets, and resorption of periodontal tissues are the noteworthy symptoms and clinicopathological features of periodontitis [3–6]. Research indicates that the effective periodontal treatment can significantly improve both oral and systemic health [7]. The primary goal of periodontitis treatment is to regenerate damaged tissue and restore the function of affected teeth. The regeneration of alveolar bone and cementum is considered as the challengings in clinic practice [8,9].

The advancement of guided tissue regeneration (GTR) has bring promising outcomes in the realm of regenerative treatment for periodontitis. The fibrous membrane is crucial in preventing the entry of epithelial cells and fibroblasts into the space for alveolar bone regeneration without disrupting the healing process of wound [10–12]. Common polymer membrane materials including poly (ε-caprolactone)

* Corresponding author. The Affiliated Stomatological Hospital of Nanjing Medical University, No.1 Shanghai Road, Gulou District, Nanjing City, Jiangsu Province, People's Republic of China.
E-mail address: xiaoqianwang@njmu.edu.cn (X. Wang).
[1] These authors contributed equally to this work.

https://doi.org/10.1016/j.mtbio.2024.101036
Received 12 January 2024; Received in revised form 6 March 2024; Accepted 19 March 2024
Available online 2 April 2024
2590-0064/© 2024 The Authors. Published by Elsevier Ltd. This is an open access article under the CC BY-NC license (http://creativecommons.org/licenses/by-nc/4.0/).

(PCL) and poly (lactic acid-co-glycolic acid) (PLGA), which have been approved by the FDA for implantation in vivo [13–15]. However, polymer membrane materials possessed suboptimal cellular response, limited osteo-conductive potential, and deficient immune microenvironment regulation because of weak surface hydrophilicity [16,17].

Graphene oxide (GO) is known for its outstanding mechanical and biological properties [18–22]. However, due to its high cytotoxicity, reduced GO (rGO) is more widely used. Most of the commonly used reducing agents are cytotoxic, so it is necessary to synthesize a new kind of more biosafe material. We successfully developed a novel nanomaterial, tea polyphenols functionalized graphene oxide (TPG), employing Tea polyphenols (TPs) for the reduction and functionalization of GO [23,24]. Experimental results have validated that TPG exhibits superior biocompatibility compared to GO, rendering it suitable for further applications in the modification of PLGA/PCL fibrous membrane materials. Electrospun nanofibers possess significant benefits, such as a substantial specific surface area and porosity, making them highly promising for applications in biomedical fields such as tissue engineering [25–27]. Moreover, nanofibers can also influence the activity of stem cells and enhance celluar adhesion, proliferation, and differentiation [28]. Therefore, we use TPG, PLGA and PCL as raw materials to synthesize new nanomaterials by electrospinning, namely nTPG/PLGA/PCL.

Macrophages polarization plays a crucial role in bone immunity and tissue regeneration through subtle regulation of cytokines [29,30]. The pro-inflammatory cytokines produced by M1 macrophages stimulate bone resorption, whereas cytokines released by M2 macrophages promote bone regeneration [29–31]. Notably, M1 polarization of macrophages is dominant during the progression of periodontitis. Promoting M2 polarization and inhibiting M1 polarization are the keys to reverse periodontal inflammation and promote periodontal regeneration and repair.

In this study, the TPG nanolayer material, successfully developed in previous studies [23], was employed to functionalize the PLGA/PCL nanofibrous membrane in the current investigation. The physicochemical and biocompatible characteristics were thoroughly examined, leading to the identification of the optimal functional nTPG/PLGA/PCL nanofibrous membrane. There has been a predominant emphasis on direct impact of polymer barrier membranes on tissue regeneration, with a relative lack of exploration into the regulatory effects and mechanisms of polymer barrier membranes on the immune microenvironment. The study further explored the regulatory effects of nTPG/PLGA/PCL fibrous membrane on the polarization of macrophages and its bone immunomodulatory properties on hPDLSCs in vitro and in vivo.

2. Materials and methods

2.1. Preparation of nTPG/PLGA/PCL fibrous membranes

PCL (80000 kD, Sigma-Aldrich) and PLGA (LA:GA = 50:50, MW = 106000, Jinan Daigang Biomaterial) were combined and stirred in HFIP (Aladdin) with a concentration of 10% (w/v) to obtain a polymer solution. TPG (tea polyphenols functional graphene oxide) was synthesized by Jiangsu Xianfeng Nanomaterial Technology Co. Ltd. To prepare composite membranes with varying TPG mass fractions (0.0%, 0.3%, 0.5%, 0.8%, 1.0%), TPG was dispersed in a PLGA/PCL solution. The resulting solution was then loaded into a 10 mL syringe fitted with a metal needle. The needle's tip was positioned 20 cm away from a collector covered with silicone paper. Applying a voltage of 14 kV to the syringe needle, the solution was dispensed at flow rate of 1 mL/h. The electrospinning process took place for 10 h under ambient conditions with a relative humidity of 50% and a room temperature. Post-electrospinning, the membranes were collected and subjected to a vacuum-drying process lasting 3 days within a desiccator. According to the different amounts of TPG added, they were named as PLGA/PCL, 0.3%TPG/PLGA/PCL, 0.5%TPG/PLGA/PCL, 0.8%TPG/PLGA/PCL, 1.0%TPG/PLGA/PCL.

2.2. Physicochemical characterization of the fibrous membranes

The morphological traits and structural features were examined under an S-4800 scanning electron microscope (SEM, Hitachi, Japan). These SEM images were measured for fiber diameter using Image J software. The chemical constituents of the membranes were evaluated by FTIR spectroscopy (VERTEX 80 V, Bruker, Germany). The mechanical properties were tested by a universal inspection machine (DZF-6020, China) at room temperature. The membranes were sliced into rectangles (4×1 cm) and stress-strain curves were recorded. The degradation rates were determined by measuring the weight loss in a physiological solution on days 0, 1, 3, 7 and 14. The samples were first weighted (W0) and then incubated in 10 mL PBS in centrifuge tubes with the rotating speed of 100 r/min. The weight of each sample was documented at pre-established time points (Wt) after drying. The remaining mass rates were then measure as $Wt/W0 \times 100\%$. The contact angle of the membrane was determined through static water contact angle measurement (Automatic Contact Angle Meter Model SL200B, China).

2.3. Cell culture

The RAW 264.7 cells line (Jiangsu Province Key Laboratory of Oral Diseases) and primary hPDLSCs were used in this study. Detailed methods are given in Supplementary Information.

2.4. Cytocompatibility of the fibrous membranes

hPDLSCs were seeded onto the membranes at a density of 2×10^4 cells/well in a 24-well plate. Following a 3-day cultivation period, cells were treated with 4% paraformaldehyde for 10 min for fixation, followed by permeabilization using 0.1% Triton X-100 (Beyotime, China) for 5 min. Subsequent to blocking with 1% bovine serum albumin (BSA, Sigma Aldrich) for 30 min, the cells were stained with rhodamine phalloidin (Beyotime, China) for cytoskeleton and 4', 6-Diamidino-2-phenylindole, dihydrochloride (DAPI, Beyotime, China) for the nucleus. The cellular structure and attachment to the membranes were examined using a confocal laser scanning microscope (CLSM, LSM 800, Carl Zeiss, Jena, Germany). The RAW 264.7 macrophages were cultured on the membranes with a density of 2×10^4 cells/well separately. Following a 3-day incubation, cells were fixed overnight with 2.5% glutaraldehyde. Subsequently, the fixed cells underwent dehydration using graded ethanol solutions (30%, 50%, 70%, 90%, and 100%) for 10 min respectively. Following dehydration, the specimens were subjected to freeze-drying and observed under SEM. In accordance with the protocol, the CCK8 assay was performed to assess the cell viability. Detailed methods were given in Supplementary Information.

2.5. In vitro regulation of immune microenvironment of macrophages

We selected *Escherichia coli (E.coli)* lipopolysaccharide (LPS) and interferon-γ (IFN-γ) as the inflammatory stimulus in this research. RAW 264.7 cells were pre-treated with the different membranes for 6 h. Subsequently, the culture medium was supplemented with or without LPS (100 ng/mL) and IFN-γ (10 ng/mL).

The macrophages polarization related genes, including M1 phenotype (TNF-α, iNOS, IL-6), M2 phenotype (Arg-1, IL-10) and osteogenic factor (BMP-2) (primers are listed in Table 1) were investigated by qRT-PCR. Moreover, cells treated for 18 h were gathered and detected by Western blotting analysis to evaluate the protein expression levels of iNOS (M1 marker) and Arg-1 (M2 marker). Alternatively, the cells were utilized for flow cytometry (BD FACSCalibur, United States) to assess the expression of CD86 (M1 marker) and CD206 (M2 marker). Besides, the concentration of anti-inflammatory cytokine (TNF-α) in the collected

Table 1
Primer sequences for qRT-PCR.

Gene	Forward Primer (5′-3′)	Reverse Primer (5′-3′)
GAPDH (M)	ATCACTGCCACCCAGAAG	TCCACGACGGACACATTG
TNF-α (M)	TCTTCTCATTCCTGCTTGTGG	GAGGCCATTTGGGAACTTCT
iNOS (M)	CAGCTGGGCTGTACAAACCTT	CATTGGAAGTGAAGCGTTTCG
IL-6 (M)	AGTTGCCTTCTTGGGACTGA	TCCACGATTTCCCAGAGAAC
Arg-1 (M)	CCAGATGTACCAGGATTCTC	AGCAGGTAGCTGAAGGTCTC
IL-10 (M)	ACTCTTCACCTGCTCCACTG	GCTATGCTGCCTGCTCTTAC
BMP-2 (M)	TGAGGATTAGCAGGTCTTTGC	GCTGTTTGTGTTTGGCTTGA
AKT1 (M)	AACAGCAGATGGCCCATACC	AACCTTTGCTGGTCCCACAT
AKT2 (M)	ACCCCCAGACCGATATGACA	CTCGGATGCTGGCTGAGTAG
C/EBP-β (M)	GAAGACGGTGGACAAGCTGA	GCTTGAACAAGTTCCGCAGG
JAK2 (M)	ACAGACAAGTGGAGCTTCGG	CAGGCCTGAAATCTGGCTCA
STAT3 (M)	TCAGCGAGAGCAGCAAAGAA	CACTACCTGGGTCGGCTTC
JNK1 (M)	CTGAAGCAGAAGCTCCACCA	CACCTAAAGGAGAGGGCTGC
JNK2 (M)	AGTGGGTTGCATCATGGGAG	TCTGCTGATGGTGTTCCCAG
p38 (M)	GTGGCCACTAGGTGGTACAG	TTCTTCAAAAGCTCAGCCCC
MyD88 (M)	AGGCATCACCACCCTTGATG	CGAAAAGTTCCGGCGTTTGT
Iκ-B (M)	CCAGTGCCTGTGACAGCTTA	CTTTCTAGCCGGGAGCAGAG
NF-κB (M)	AACAGCAGATGGCCCATACC	AACCTTTGCTGGTCCCACAT
GAPDH (H)	CGCTCTCTGCTCCTCCTGTT	CCATGGTGTCTGAGCGATGT
ALP (H)	GACCCTTGACCCCCACAAT	GCTCGTACTGCATGTCCCCT
Runx-2 (H)	GGAGTGGACGAGGCAAGAGTTT	AGCTTCTGTCTGTGCCTTCTGG
COL-1 (H)	AGAACAGCGTGGCCT	TCCGGTGTGACTCGT
OCN (H)	GGCAGCGAGGTAGTGAAGAG	GATGTGGTCAGCCAACTCGT
CEMP-1 (H)	GGGCACATCAAGCACTGACAG	CCCTTAGGAAGTGGCTGTCCAG
CAP (H)	CTGCGCGCTGCACATGG	GCGATGTCGTAGAAGGTGAGCC
RANKL (H)	GGCTCATGGTTAGATCTGGC	TGACCAATACTTGGTGCTTCC
OPG (H)	TCAAGCAGGAGTGCAATCG	AGAATGCCTCCTCACACAGG

M = murine, H = human.

induction medium was detected with corresponding ELISA kits (Multi Sciences, China). Detailed methods are given in Supplementary Information.

In order to explore the regulation of RAW 264.7 polarization related signal pathway by nTPG/PLGA/PCL nanofibrous membranes, the qRT-PCR was used to screen the related genes that might be associated with the signaling pathway. The key genes selected for the related signaling pathways were AKT1, AKT2, C/EBP-β of PI3K/Akt signaling pathway; JAK2 and STAT3 of JAK-STAT signal path; JNK1/2, p38 of TGF-β signaling pathway and MyD88, NF-κB, Iκ-B of TLR4/NF-κB signaling pathway. Western blotting further confirmed the expression levels of the differentially expressed gene-related proteins (p-PI3K/PI3K, p-AKT/AKT, p-IκBα/IκBα, and p-NF-κB/NF-κB) screened in the previous step. Based on the above research results, the signal pathways related to RAW 264.7 polarization regulated by nTPG/PLGA/PCL nanofibrous membranes were preliminarily identified. The membranes were administered for 24 h, with or without the addition of the PI3K/Akt activator 740 Y-P (25 μg/mL) or the NF-κB activator phorbol myristate acetate (PMA, 1 μM). Subsequently, the expression of relevant proteins was reassessed by Western blotting. Finally, the molecular mechanism of nTPG/PLGA/PCL regulating RAW 264.7 polarization was confirmed. The antibodies we used were in Supplementary Information.

2.6. The direct regulation of nTPG/PLGA/PCL fibrous membranes on hPDLSCs osteogenesis and cementogenesis

hPDLSCs (2×10^5 cells/well) were seeded onto various fibrous membranes and cultured in osteogenic differentiation medium (OS, growth medium supplemented with 0.1 μM dexamethasone, 10 mM β-glycerophosphate, and 50 μM ascorbic acid) for 7 and 14 days. After 7 days of incubation with different membranes, the gene expression of factors related to the osteogenic genes (ALP, Runx-2, COL-1, OCN), cementogenetic genes (CEMP-1, CAP) and osteoclast genes (RANKL, OPG) (primers are listed in Table 1) were analyzed by qRT-PCR.

Additionally, after 14 days of incubation with different membranes, the cells were gathered and used for Western blotting. The protein levels of ALP (Abcam, #ab229126, dilution ratio: 1:1000), Runx-2 (Cell Signaling Technology, #12556, Rabbit mAb, dilution ratio: 1:1000), COL-1 (Bioworld, #BS60771, dilution ratio: 1:800), OCN (Abcam, #ab133612, dilution ratio: 1:500), CEMP-1 (Abcam, #ab134231, dilution ratio: 1:500) and CAP (Santa Cruz, #sc-53947, dilution ratio: 1:400) were evaluated by Western blotting.

The following research, we selected a fibrous membrane with appropriate TPG concentration for subsequent study based on the above research results.

2.7. The indirect regulation of nTPG/PLGA/PCL fibrous membranes on hPDLSCs osteogenesis and cementogenesis by regulating the polarization of RAW 264.7

The co-culture system of macrophages and hPDLSCs was developed through the conditioned medium. RAW 264.7 cells were pre-incubated with the different membranes for 6 h. Then, LPS (100 ng/mL) and IFN-γ (10 ng/mL) were or were not added to the culture medium. After 18 h of incubation, the media of RAW 264.7 cells were collected respectively. Basal culture medium was then blended with the obtained supernatant in a 3:1 ratio to create the conditioned medium (CM) for subsequent experiments. hPDLSCs were seeded into 96-well plates at a density of 1×10^4 cells per well and categorized into four groups: 1) control group, cells cultured in normal culture medium; 2) LPS group, cells cultured in CM of RAW 264.7 cells that were treated with LPS and IFN-γ; 3) LPS + PLGA/PCL group, cells cultured in CM of RAW 264.7 cells that were treated with LPS, IFN-γ and PLGA/PCL; 4) LPS+0.5% TPG/PLGA/PCL group, cells cultured in CM of RAW 264.7 cells that were treated with LPS, IFN-γ and 0.5%TPG/PLGA/PCL. After being cultured for 24 h, the culture medium was substituted with a distinct CM based on the grouping conditions. On day 1, 3, 5 and 7, hPDLSCs proliferation and viability were measured by the CCK-8.

To assess how macrophages regulate osteo/cementogenic differentiation of hPDLSCs in response to nTPG/PLGA/PCL fibrous membranes, cells were seeded in 6-well plates (2×10^5 cells/well). Subsequently, the cells were cultured with the respective CM supplemented with osteogenic differentiation medium. After 7 days, the mRNA expression levels of the osteogenic genes (ALP, Runx-2, COL-1, OCN), cementogenetic genes (CEMP-1, CAP) and osteoclast genes (RANKL, OPG) (primers are listed in Table 1). After 14 days, the protein levels of ALP, Runx-2, COL-1, OCN, CEMP-1 and CAP were evaluated by Western blotting. After 7 days of incubation, ALP activity was assessed using an Alkaline Phosphatase Assay Kit (Beyotime Biotechnology, China). Additionally, cells were stained with the BCIP/NBT Alkaline Phosphatase Color Development Kit (Jiancheng Bioengineering Institute, China) according to the protocol. Optical density (OD) values at 520 nm were recorded, and the wells were inspected using an optical microscope (Leica, Germany) and photographed with a scanner (EOS 6D, Japan). Furthermore, cells were cultured in osteogenic differentiation medium for 28 days and then stained with 2% alizarin red S (ARS, Leagene, China) solution for 5 min. Following three washes with PBS buffer, plates were examined using an optical microscope (Leica, Germany). Mineralized nodules stained by ARS were dissociated with 10% (w/v) cetylpyridinium chloride (Sigma-Aldrich, China), and absorbance was measured at 562 nm for quantification.

2.8. The in-vivo periodontal regeneration potential of the nTPG/PLGA/PCL membranes in a rat periodontitis model

All animal experiments were approved by the ethics committee of Nanjing Medical University. Twenty-four six-week-old Sprague Dawley

(SD) rats (male, 100–150 g) were chosen to construct periodontal defect models. The rats were randomly divided into three groups (n = 8 for each group): 1) control group, only with flap surgery treatment, after surgery without any membranes treatment; 2) PLGA/PCL group, after surgery with PLGA/PCL membranes; 3) 0.5%TPG/PLGA/PCL group, after surgery with 0.5%TPG/PLGA/PCL membranes. After general anesthesia, the maxillary left second molar of the rat was ligated with a 4-0 silk suture for 21 days. Upon the establishment of the periodontitis model, the surgical sutures were extracted, then a full-thickness flap was elevated from the first molar to the third. All granulation tissue was removed from the pocket, root the fibrous surface calculus and other irritants meticulously were also scraped off. Making sure membrane covered the entire bone defect when placed, extending 1 mm beyond the defect's edge. Finally, the surgery wounds were fixed with periodontal dressing (Bonanga, China). At 14 and 28 days postsurgery, the rats were euthanized, and the entire upper jaw, including the gingival palate, bone, and mucosal tissues, were cut off. All samples underwent a thorough wash with distilled water and were promptly deposited in a 4% paraformaldehyde solution for subsequent analysis.

2.9. Micro-CT analysis

To analyze bone remodeling, a micro-CT (SCANCO Medical AG, Switzerland) at the intensity of 55 kVp, 83 μA, 6 W was used to scan the specimens. CT analysis software were employed to reconstruct the images, enabling 3D visualization and evaluation. The ratio of alveolar bone crest (ABC) to tooth apex (TP) and cementoenamel junction (CEJ) to tooth apex (ABC-TP/CEJ-TP) between first and second molars was calculated. The lingual side of the second molar was selected, and the assessment of bone regeneration was conducted through nalyzing and calculating the percentages of bone volume/tissue volume (BV/TV).

2.10. Histological analysis

The fixed rats maxillary were decalcified with disodium ethylenediamine tetraacetate (EDTA) and the process was carried out by constant temperature shaker. Afterwards, the specimens underwent dehydration using a series of ethanol solutions in a dehydrator. Following the transparent treatment with xylene, the specimens were embedded in paraffin to obtain paraffin sections with a thickness of 4 μm. Hematoxylin and Eosin (H&E) as well as Masson trichrome staining were conducted under constructions.

Immunohistochemistry (IHC) and Immunofluorescence (IF) staining were performed to evaluate periodontal tissue regeneration complied with the manufacturer's protocols. The primary antibodies included OCN (Servicebio, GB11233, 1:50), COL-1 (proteintech, AG6281, 1:100), RUNX-2 (Affinity, AF5186, 1:200), BMP-2 (abcam, ab284387, 1:200).

To appraise osteoclastogenesis, tartrate-resistant acid phosphatase (TRAP) staining was performed using a TRAP dye solution kit (Servicebio, GB1050) to identify TRAP-positive cells. The staining of specimens was scanned by a panorama Scanner (3DHISTECH, Hungary). All the data were measured by Image-Pro Plus 6.0 (Media Cybemetics, USA).

In order to detect phenotype switching of macrophages, in vivo, the tissue sections were incubated with primary antibodies of iNOS (Abcam, ab178945, 1:200), CD68 (Abcam, ab201340, 1:200), CD163 (Sevicebio, GB113109,1:200). The iNOS positive cells (an M1 marker) and CD163 positive cells (an M2 marker) were applied by the secondary antibody with red fluorescently (Invitrogen, A21428, 1:200) and the were CD68 positive cells (a universal macrophage marker) applied by the secondary antibody with green fluorescently (Invitrogen, A11008, 1:200). The fluorescent images were captured by fluorescence microscope, and the number of CD163 + $CD68^+$ cells and iNOS + $CD68^+$ cells in the defects area was measured by Image J software.

2.11. Statistical analysis

All quantitative data were expressed as mean ± standard deviation (SD). Variances between more than two groups were compared by one-way ANOVA, and differences between two groups were analyzed by two-way *t*-test. Statistical analysis was performed using GraphPad Prism 8.0 software. $P < 0.05$ was set as statistically significant difference.

3. Results

3.1. Characterization of the fibrous membranes

The surface morphology of nTPG/TPG/PLGA/PCL membranes was examined by SEM (Fig. 1A). The top right section of the images displayed comprehensive photographs of the five membranes. The SEM results indicated that TPG (highlighted by red arrows) was assembled in the membrane fibers successfully. All fibers displayed a uniform and smooth morphology, without beads or broken strands. Mean diameters were measured as follows: 1.40 μm (PLGA/PCL), 1.71 μm (0.3%TPG/PLGA/PCL), 1.58 μm (0.5%TPG/PLGA/PCL), 2.70 μm (0.8%TPG/PLGA/PCL) and 1.70 μm (1.0%TPG/PLGA/PCL), respectively (Fig. 1B).

The surface chemical properties and characteristic functional groups of nTPG/PLGA/PCL membranes were evaluated by the FTIR method (Fig. 1C). As revealed by the spectrum of the PLGA/PCL membrane, the frequency at 2950 cm^{-1} was assigned to $–CH_3$ vibration. The peak at 1368 cm^{-1} was attributed to the $–CH_2$ bending vibration, and the peaks at 735 cm^{-1} belonged to the –CH bending vibrations. Furthermore, the prominent peak at 1728 cm^{-1} was corresponding to the absorption by –C═O, and the frequencies at 1163 cm^{-1} and 1088 cm^{-1} were related to –C–O stretching vibration. The peaks of these TPG-doped membranes closely resembled those of the original PLGA/PCL, which showed that the chemical properties were not affected by the electrospinning.

The progressive degradation of the membranes was monitored through weight measurements (Fig. 1D). All groups experienced substantial weight loss during the initial week. In the second week, the degradation rate of the fibrous membranes slowed down, leading to a gradual dissolution. Notably, the PLGA/PCL membrane group displayed more weight loss compared to the nTPG/PLGA/PCL membrane groups. These results affirmed that the incorporation of TPG decelerated the degradation rate of the fiber membranes.

The surface wettability of the membranes was assessed by measuring the water contact angle (WCA) (Fig. 1E). The results indicated a significantly higher hydrophilicity in nTPG/PLGA/PCL compared to PLGA/PCL, suggesting that the addition of TPG could enhance the hydrophilicity of the pristine PLGA/PCL membranes. Among them, 0.8% TPG/PLGA/PCL exhibited the most favorable surface wettability.

The mechanical properties of the membranes were evaluated by tensile testing (Fig. 1F). Comparison to PLGA/PCL, the nTPG/PLGA/PCL exhibited a significant increase in tensile strength and Young's modulus, particularly in the 0.5%TPG/PLGA/PCL group.

3.2. Cytocompatibility of the fibrous membranes

The separation and extraction process of hPDLSCs was illustrated in Fig. 5A. Flow cytometric analysis demonstrated that hPDLSCs exhibited positive expression of mesenchymal stem cell (MSC) markers CD73 and CD90, and showed negative expression of hematopoietic stem cell markers CD34 and CD45 (Fig. 5B). The CCK-8 assay was performed to assess the cytotoxic impact of fibrous membranes. After cultivation for 1, 3, 5 and 7 days, both RAW 264.7 (Fig. 2B) and hPDLSCs (Fig. 5C) showed high viability, with no significant differences observed among different groups. After 3 days of culture, RAW 264.7 extended the pseudopods and exhibited robust growth on the fibrous membranes as observed by SEM (Fig. 2A). In addition, cytoskeleton (Factin) staining reflected the morphology of hPDLSCs on various fibrous membranes (Fig. 5D). Results showed hPDLSCs adhered to all the membranes and

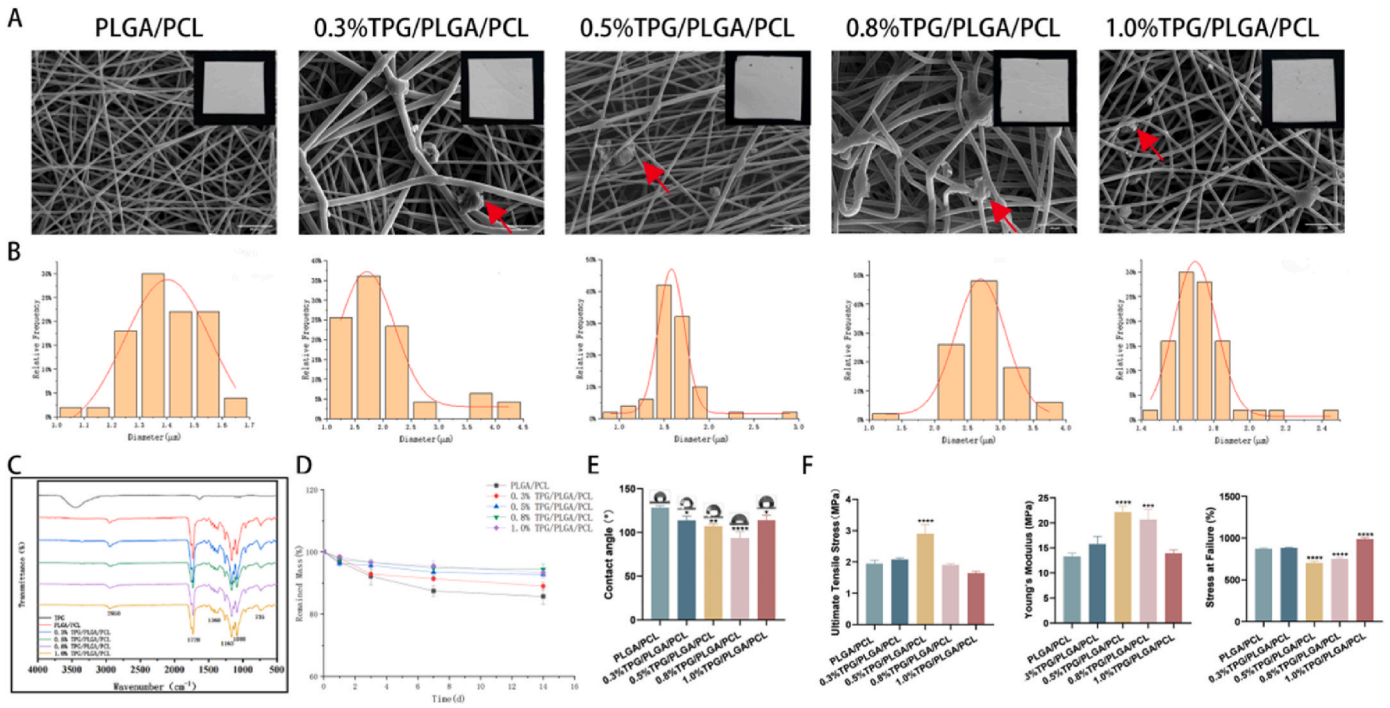

Fig. 1. Structure and characterization of five electrospinning membranes (PLGA/PCL, 0.3% TPG/PLGA/PCL, 0.5%TPG/PLGA/PCL, 0.8%TPG/PLGA/PCL, 1.0%TPG/PLGA/PCL). (A) SEM images and gross photographs of different fibrous membranes (red arrow is TPG). (B) Analysis of diameter distribution of different fibrous membranes. (C) FTIR spectrum of fibrous membranes. (D) Degradation curve of fibrous membranes. (E) Hydrophilicity of fibrous membranes. (F) Extreme tensile strength, Young's modulus and fracture strain of fibrous membranes. Variances were compared by one-way ANOVA. n ≥ 3. Scale bar = 30 μm $^{*}P < 0.05$, $^{**}P < 0.01$, $^{****}P < 0.001$ compared with PLGA/PCL. (For interpretation of the references to colour in this figure legend, the reader is referred to the Web version of this article.)

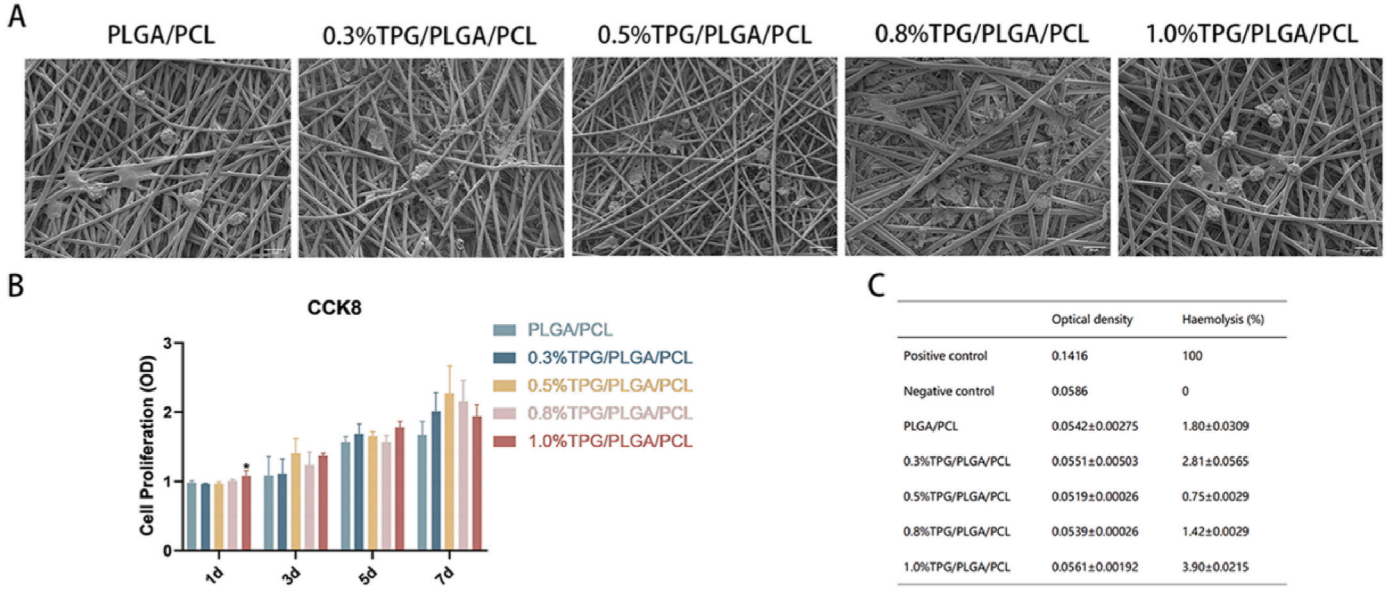

	Optical density	Haemolysis (%)
Positive control	0.1416	100
Negative control	0.0586	0
PLGA/PCL	0.0542±0.00275	1.80±0.0309
0.3%TPG/PLGA/PCL	0.0551±0.00503	2.81±0.0565
0.5%TPG/PLGA/PCL	0.0519±0.00026	0.75±0.0029
0.8%TPG/PLGA/PCL	0.0539±0.00026	1.42±0.0029
1.0%TPG/PLGA/PCL	0.0561±0.00192	3.90±0.0215

Fig. 2. Cytocompatibility of the fibrous membranes. (A) SEM images of RAW 264.7 cultured on fibrous membranes. (B) Cell viability after cultivation with different fibrous membranes. (C) Red blood cell hemolysis test. Variances were compared by one-way ANOVA. n ≥ 3. Scale bar = 10 μm $^{*}P < 0.05$. (For interpretation of the references to colour in this figure legend, the reader is referred to the Web version of this article.)

extended across the elongated fibers with well-defined cytoskeletal structures. Furthermore, the membranes' biocompatibility was assessed by erythrocyte hemolysis test (Fig. 2C). These results showed that the hemolysis rate of all fibrous membranes was less than 5%, which meet the requirements for hemolysis experiments involving medical implant materials. These data affirmed the biocompatibility of nTPG/PLGA/PCL was biological safe as the supportive attachment surfaces for cellular growth.

3.3. *In vitro* regulation of immune microenvironment of macrophages

Upon stimulation with LPS and IFN-γ, nTPG/PLGA/PCL demonstrated remarkable inhibition of RAW 264.7 polarization towards inflammatory phenotypes. The flow cytometry was utilized to evaluate the

expression of CD86, which serves as a surface marker indicative of M1-phenotype macrophages. The results (Fig. 3A) indicated that 0.5%TPG/PLGA/PCL significantly inhibited the up-regulation of CD86 expression induced by LPS and IFN-γ. While the change of expression level of the M2 marker CD206 in RAW 264.7 cells was not significant. According to the qRT-PCR results (Fig. 3B), inflammatory stimulation resulted in an extremely high expression of iNOS, TNF-α, and IL-6, while nTPG/PLGA/PCL significantly attenuated this effect, especially the 0.5%TPG/PLGA/PCL group. In addition, because of the effect of 0.5%TPG/PLGA/PCL and 0.8%TPG/PLGA/PCL, the expression of Arg-1, IL-10 and BMP-2 were higher than those of the other group. Western blotting detected the protein expression of the M2 maker Arg-1 and M1 maker iNOS (Fig. 3C), indicating that LPS and IFN-γ increased the production of M1 maker iNOS and decreased the formation of M2 maker Arg-1, while 0.5%TPG/PLGA/PCL inhibited these phenotypic transitions. ELISA result (Fig. 3D) further confirmed the effect of 0.5%TPG/PLGA/PCL on reducing the concentration of the pro-inflammatory factor TNF-α.

In summary, the aforementioned results highlighted the superior performance of 0.5%TPG/PLGA/PCL in RAW 264.7 phenotypic transition regulation than other fibrous membranes in our research. Consequently, 0.5%TPG/PLGA/PCL was selected for the subsequent research.

To delve into the mechanism underlying the regulation of macrophages by 0.5%TPG/PLGA/PCL membranes, q-PCR and Western blotting were performed for investigation. LPS and IFN-γ treatment up-regulated genes (NF-κB,MyD88, C/EBPβ, AKT1, AKT2, P38, JAK2, and STAT3) and proteins (p-PI3K/PI3K, p-AKT/AKT, p-IκBα/IκBα, and NF-κB (p65)) in RAW 264.7 macrophages. Notably, these changes were significantly decreased by 0.5%TPG/PLGA/PCL (Fig. 4A and B). When RAW 264.7 cells were pre-treated with pathway activators, the inhibited effect was partially hindered by the PI3K/AKT activator 740 Y-P and the NF-κB activator PMA (Fig. 4C). These findings indicated that 0.5%TPG/PLGA/PCL might inhibit M1 polarization of macrophages via restraining the activation of PI3K/AKT and NF-κB signaling pathways.

3.4. The direct regulation of 0.5%TPG/PLGA/PCL fibrous membranes on hPDLSCs osteogenesis and cementogenesis

The hPDLSCs were inoculated with PLGA/PCL and 0.5%TPG/PLGA/PCL fibrous membranes respectively, the mRNA levels of ALP, RUNX-2, COL-1, OCN, CEMP-1, CAP, RANKL and OPG were detected by qRT-PCR on day 7 (Fig. 6A). The expressions of osteogenic gene (ALP) and cementoblastic genes (CEMP-1) were significantly increased in contrast

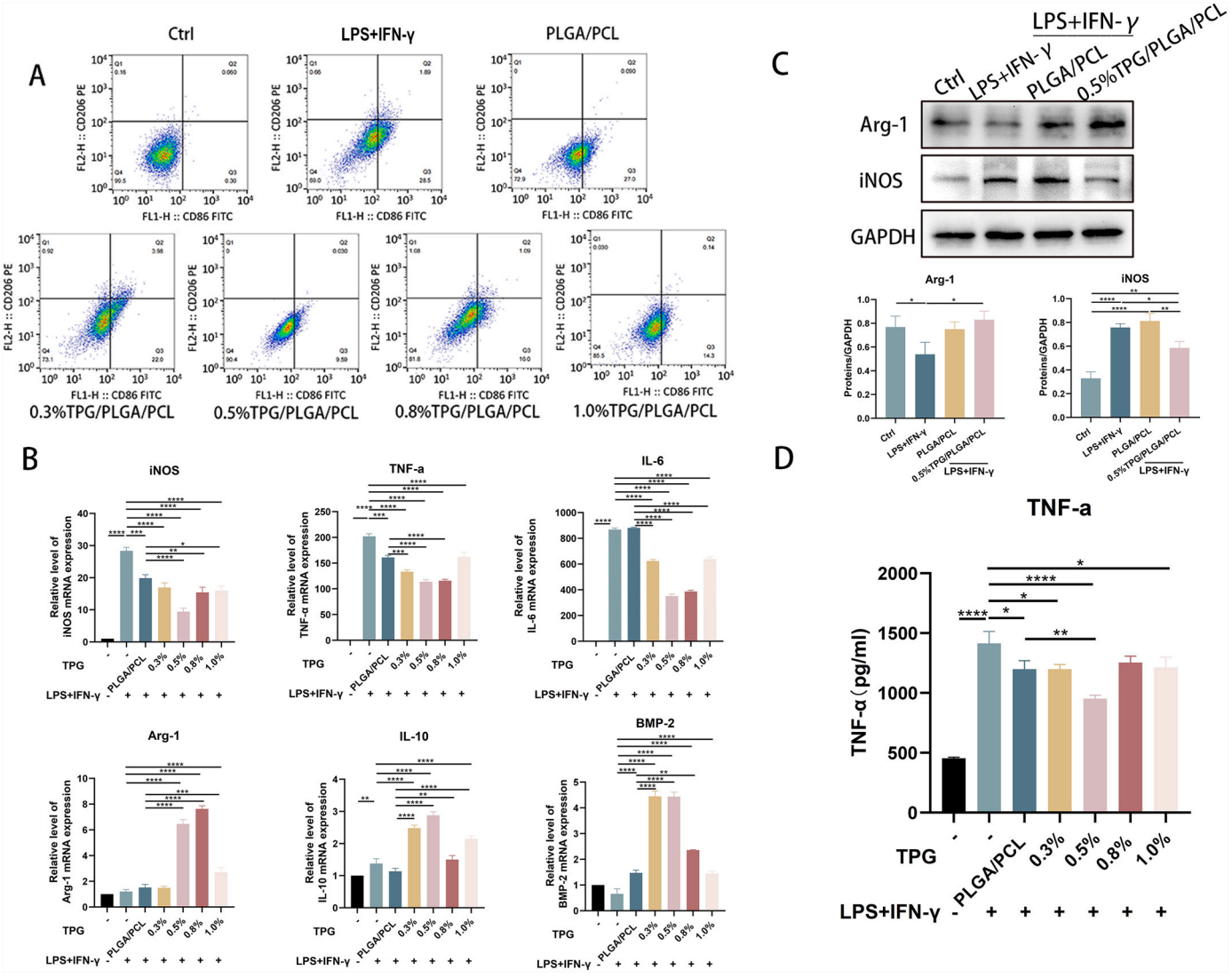

Fig. 3. Regulation of nTPG/PLGA/PCL nanofibrous membranes on polarization of RAW 264.7 macrophages. (A) The phenotype of RAW 264.7 was analyzed by flow cytometry. (B) The expression of RAW 264.7 related genes (iNOS, TNF-α, IL-6, Arg-1, IL-10, BMP-2) was analyzed by qRT-PCR. (C) Western blotting analysis of RAW 264.7 related protein expression (iNOS, Arg-1) (D) The content of inflammatory cytokines (TNF-α) was measured by ELISA. Variances were compared by one-way ANOVA. $n \geq 3$. $^{*}P < 0.05$, $^{**}P < 0.01$, $^{***}P < 0.001$, $^{****}P < 0.001$.

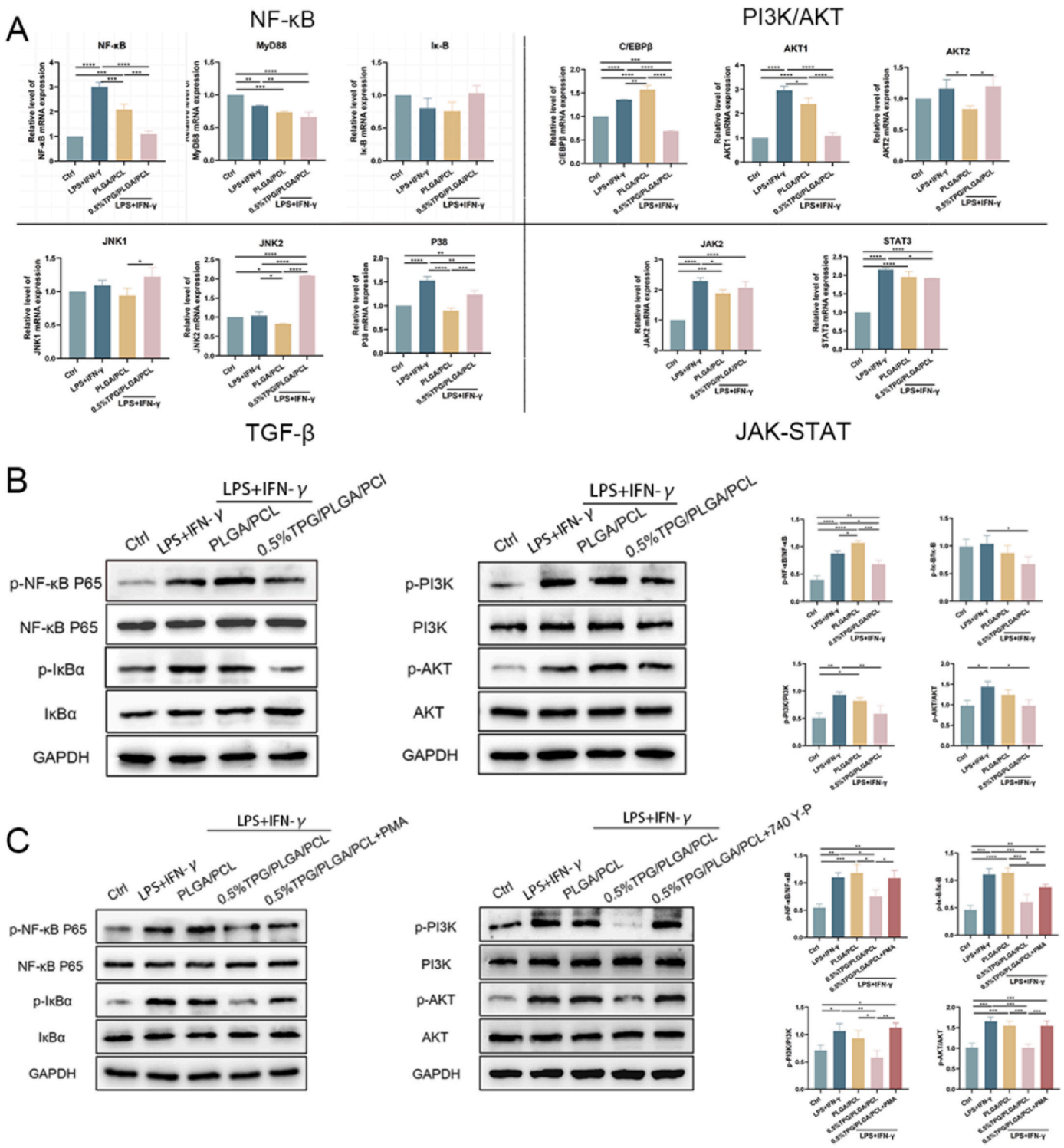

Fig. 4. Regulation of RAW 264.7 polarization related signaling pathways by 0.5%TPG/PLGA/PCL fibrous membranes. (A) qRT-PCR analysis of possible signaling pathways (NF-κB, PI3K/AKT, TGF-β, JAK-STAT) related gene expression. (B) Western blotting analysis of NF-κB and PI3K/AKT pathways related protein expression. (C) Western blotting analysis of NF-κB and PI3K/AKT signaling pathways related proteins expression after treatment with the activator. Variances were compared by one-way ANOVA. n ≥ 3. *$P < 0.05$, **$P < 0.01$, ***$P < 0.001$, ****$P < 0.001$.

to the PLGA/PCL group, while the ratio of RANKL/OPG decreased following treatment with both fibrous membranes. Other genes (RUNX-2, COL-1, OCN, CAP) did not show significantly enhancement. Additionally, the protein (CEMP-1) level of 0.5%TPG/PLGA/PCL group was significantly higher than that of control group on day 14 by Western blotting (Fig. 6B).

3.5. The indirect regulation of 0.5%TPG/PLGA/PCL fibrous membranes on hPDLSCs osteogenesis and cementogenesis by regulating the polarization of RAW 264.7

Initially, the CCK8 results (Fig. 7A) showed that CM induced by 0.5% TPG/PLGA/PCL promoted hPDLSCs growth on day 5 compared to the control group. On day 1, 3 and 7, no significant differences was observed

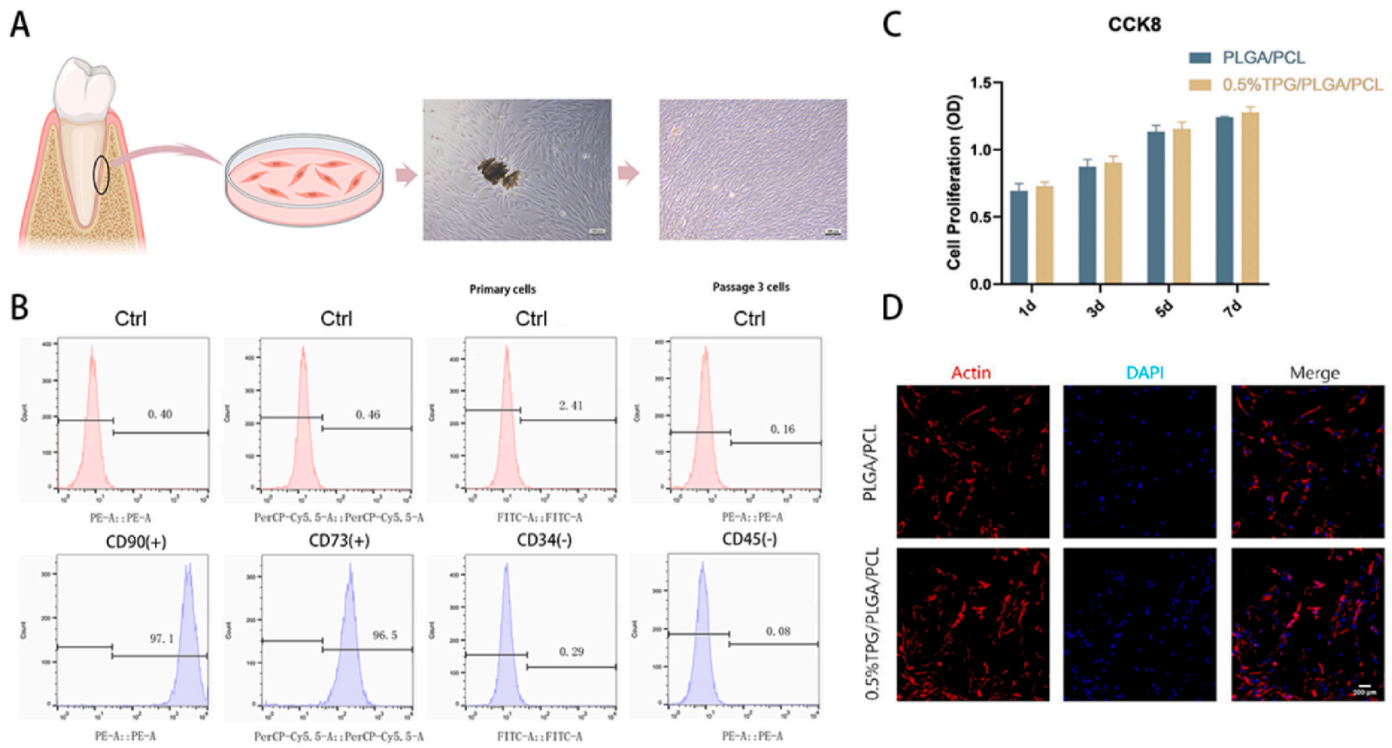

Fig. 5. Primary cell extraction of hPDLSCs and cytocompatibility of fibrous membranes. (A) Primary hPDLSCs cells were extracted. (B) Identification of hPDLSCs surface molecules by flow cytometry. (C) Cell viability after cultivation with different fibrous membranes. (D) Cytoskeleton staining of hPDLSCs cultured on fibrous membranes (red, cytoskeleton stained with Rhodamine fluorescein. blue, nucleus stained with DAPI). Variances were compared by two-way *t*-test. n ≥ 3. Scale bar = 200 μm. (For interpretation of the references to colour in this figure legend, the reader is referred to the Web version of this article.)

among these groups. Therefore, overall, none of the three CM types had a negative effect on cell proliferation. Combined with the regulatory effect on RAW 264.7 CM, 0.5%TPG/PLGA/PCL significantly up-regulated the mRNA (Fig. 7B) and protein (Fig. 7C) levels of ALP, COL-1, RUNX-2, OCN, CEMP-1 and CAP. The analysis of ALP activity and ALP staining test exhibited that 0.5%TPG/PLGA/PCL group had higher alkaline phosphatase activity (Fig. 7D). Remarkably, even in an inflammatory microenvironment, the influence of 0.5%TPG/PLGA/PCL accelerated the mineralization process, with visible calcium nodules in hPDLSCs. On day 28, the ARS test was performed to investigate the impact of the fibrous membranes on the formation of mineralized nodules, with the calcium nodules appearing red (Fig. 7E). The corresponding CPC quantitative histogram was presented on the right and the results showed 0.5%TPG/PLGA/PCL group formed more mineralized nodules. Furthermore, we also evaluated the expression of factors related to the osteoclastic activity, including RANKL and OPG in hPDLSCs. We found that the addition of 0.5% TPG to PLGA/PCL resulted in a down-regulation of RANKL expression and an up-regulation of OPG expression in hPDLSCs through modulating macrophages CM (Fig. 7B).

In conclusion, 0.5%TPG/PLGA/PCL can directly promote the differentiation of hPDLSCs cementoblast and inhibit the activities of osteoclast. In addition, the osteogenic activity of hPDLSCs can be effectively enhanced by macrophages CM, indicating that 0.5%TPG/PLGA/PCL promotes bone and cementum regeneration in vitro.

3.6. The promotion of alveolar bone and periodontal ligament repair by 0.5%TPG/PLGA/PCL fibrous membrane in vivo

An alveolar bone defect rat model was induced by ligation of the first molar to assess to assess alveolar regeneration. After 21 days of modeling, flap surgeries were conducted in all groups. Subsequently, the PLGA/PCL group and 0.5%TPG/PLGA/PCL group were implanted with corresponding fibrous membranes. In the control group, significant alveolar bone loss and root bifurcation were evident. In contrast, the 0.5%TPG/PLGA/PCL group demonstrated higher bone height compared to other groups at all-time points (Fig. 8A). At the time points of 14 and 28 days after surgery, the ratio of ABC-TP/CEJ-TP in the 0.5%TPG/PLGA/PCL group surpassed that of the control group and PLGA/PCL group, indicating a significant increase in alveolar bone height (Fig. 8B). Moreover, the BV/TV of the palatal lateral root bifurcation of the maxillary second molar in rats in the 0.5%TPG/PLGA/PCL group demonstrated a notable increase compared to the control and PLGA/PCL groups, facilitating alveolar bone reconstruction (Fig. 8C). These findings suggested that 0.5%TPG/PLGA/PCL fibrous membrane contributed to enhanced alveolar bone regeneration.

HE staining on the gingival tissue of rats was performed to examine inflammation and tissue healing. In the control group, the alveolar bone was significantly lost, and a large area of necrosis was observed below the alveolar bone. The nucleus pyknosis and fragmentation of the necrotic area disappeared, and a large number of inflammatory cell infiltrations were observed. In the PLGA/PCL group, the overall structure of the periodontal tissue was abnormal, with noticeable hyperplasia and thickening of the gingival epithelium. Each layer of the epithelium showed increased cell volume, and the spinous layer displayed significantly proliferation. While in the 0.5%TPG/PLGA/PCL group, the epithelium resembled normal epithelium, with regularly arranged gingival epithelial cells, reduced infiltration of inflammatory cells, and evident new bone formation (Fig. 9A). Masson staining vividly illustrated functionally oriented periodontal ligament fibers, and collagen fibers were regenerated in each group, with the 0.5%TPG/PLGA/PCL group showing the most pronounced regeneration. The arrangement of new periodontal ligament tissue formed in the control group was more cluttered than that of the other groups (Fig. 9B).

Immunohistochemistry-positive staining of OCN expressions in the 0.5%TPG/PLGA/PCL group was more apparent than that in the control group (Fig. 10A–C). We assessed alveolar bone destruction by TRAP

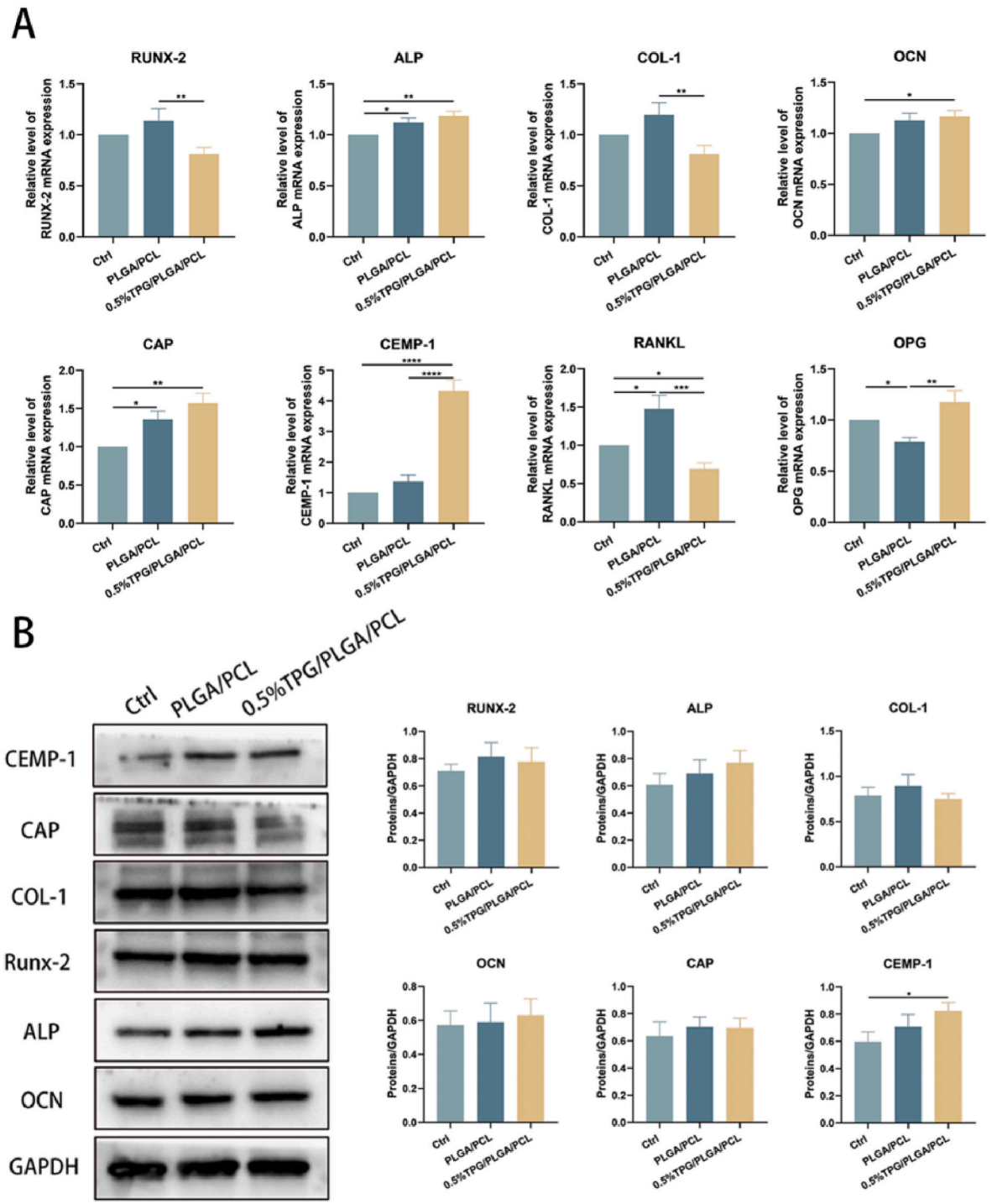

Fig. 6. The direct regulation of nTPG/PLGA/PCL fibrous membranes on hPDLSCs. (A) qRT-PCR analysis of hPDLSCs osteogenesis (ALP, Runx-2, COL-1, OCN), cementogenesis (CEMP-1, CAP) and osteoclast (RANKL, OPG) related gene expression. (B) Western blotting analysis of hPDLSCs osteogenesis (ALP, Runx-2, COL-1, OCN), cementogenesis (CEMP-1, CAP) related protein expression. Variances were compared by one-way ANOVA. n ≥ 3. $^{*}P < 0.05$, $^{**}P < 0.01$, $^{***}P < 0.001$, $^{****}P < 0.001$.

staining. In the control group, numerous osteoclasts (Fig. 10A) were observed, creating resorption lacunae in the interdental spaces between the first and second molars. The count of TRAP-positive osteoclasts in both the control group and the PLGA/PCL group was notably elevated compared to that observed in the 0.5%TPG/PLGA/PCL group (Fig. 10E). The expression of COL-1 could be detected in new fibrous tissue, normal periodontal ligament fibers, and mineralized bone tissue in each group, while the 0.5%TPG/PLGA/PC group was higher than that in the control group and PLGA/PCL group. (Fig. 10A,D). Immunofluorescence staining also showed increased expression of RUNX-2 after implantation of 0.5% TPG/PLGA/PCL compared with the control group (Fig. 10B–F). The cementum marker BMP-2 was also tested. Based on the current immunohistochemical images observed, the positive areas of BMP-2 in 0.5% TPG/PLGA/PCL group were the most obvious compared with the control group and PLGA/PCL group (Supplementary Figure 4).

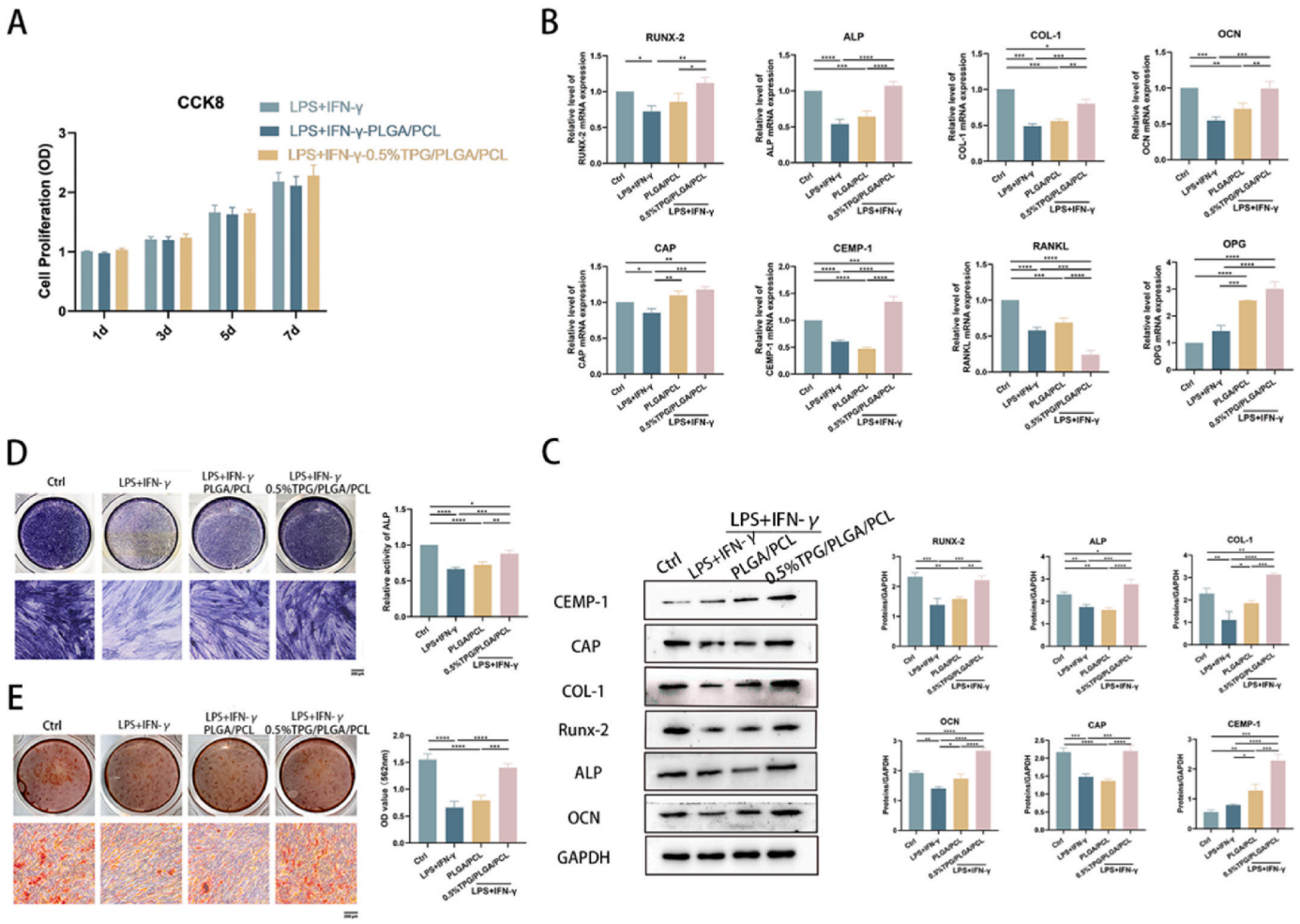

Fig. 7. The indirect regulation of nTPG/PLGA/PCL fibrous membranes on hPDLSCs by regulating the polarization of RAW 264.7. (A) The effects of RAW 264.7 culture medium on hPDLSCs cell viability. (B) qRT-PCR analysis of hPDLSCs osteogenesis (ALP, Runx-2, COL-1, OCN), cementogenesis (CEMP-1, CAP) and osteoclast (RANKL, OPG) related gene expression. (C) Western blotting analysis of hPDLSCs osteogenesis (ALP, Runx-2, COL-1, OCN), cementogenesis (CEMP-1, CAP) related protein expression. (D) ALP staining and ALP activity detection. (E) Alizarin red staining and CPC quantitative analysis of calcium content. Variances were compared by one-way ANOVA. n ≥ 3. Scale bar = 200 μm $^{*}P < 0.05$, $^{**}P < 0.01$, $^{***}P < 0.001$, $^{****}P < 0.001$. (For interpretation of the references to colour in this figure legend, the reader is referred to the Web version of this article.)

3.7. 0.5%TPG/PLGA/PCL regulates the macrophage polarization in experimental periodontitis rats

Immunofluorescence showed the polarization of macrophages in periodontal ligament. At the immunohistochemistry (Fig. 11A), the expression of CD163 + $CD68^{+}$ in the 0.5%TPG/PLGA/PCL group was higher than that in the control group and PLGA/PCL group while there were fewer iNOS + $CD68^{+}$ cells in the 0.5%TPG/PLGA/PCL group (Fig. 11B). In vivo results showed that 0.5%TPG/PLGA/PCL inhibited M1 polarization and promoted M2 polarization of macrophages, which were consistent with the results in vitro.

4. Discussion

Based on our previous investigations [23], we developed nTPG/PLGA/PCL fibrous membranes by electrospinning for periodontal tissue regeneration. Comprehensive characterization of physicochemical properties and cytocompatibility was undertaken. The efficacy of this kind of fibrous membranes in periodontal tissue regeneration and modulating the immune-microenvironment proved in vitro and in vivo.

The prepared nTPG/PLGA/PCL fibrous membranes presented as smooth morphology with a uniform distribution of diameters. The SEM analysis revealed a relatively even dispersion of TPG nanoparticles, indicating TPG nanoparticles were successfully encapsulated in fibrous membrane. The filamentous fibrous membrane, characterized by its high porosity, closely mimiced the intricate structure of the extracellular matrix. Additionally, the membrane provided ample structural space conducive to fostering osteoblast differentiation [32]. The addition of TPG nanoparticles led to a slight increase in diameter, possibly attributed to the higher polymer concentration and viscosity [33]. The FTIR spectra of the membranes with different concentration of TPG exhibited similar characteristic peaks to the original PLGA, suggesting no significant alterations in functional groups or chemical features [34]. Uncontrolled degradation rates and the inherent low mechanical strength of the membrane will pose risks of spacial support loss [35]. To mitigate this concern, incorporating TPG in the membrane retards its degradation, thereby preserving the space for bone formation over an extended period. Notably, surface wettability emerges as a crucial factor in influencing cell adhesion, growth and proliferation. The introduction of TPG improved the hydrophilicity of the PLGA/PCL fibrous membrane due to the presence of numerous hydrophilic groups on GO surface. Additionally, according to previous studies [36], the membrane could be soaked in the medium overnight to improve hydrophilicity and provide suitable surface wettability for cell adhesion and diffusion. Hotchkiss et al. reported that macrophages cultured on hydrophilic surfaces demonstrated a greater potential for differentiation toward the

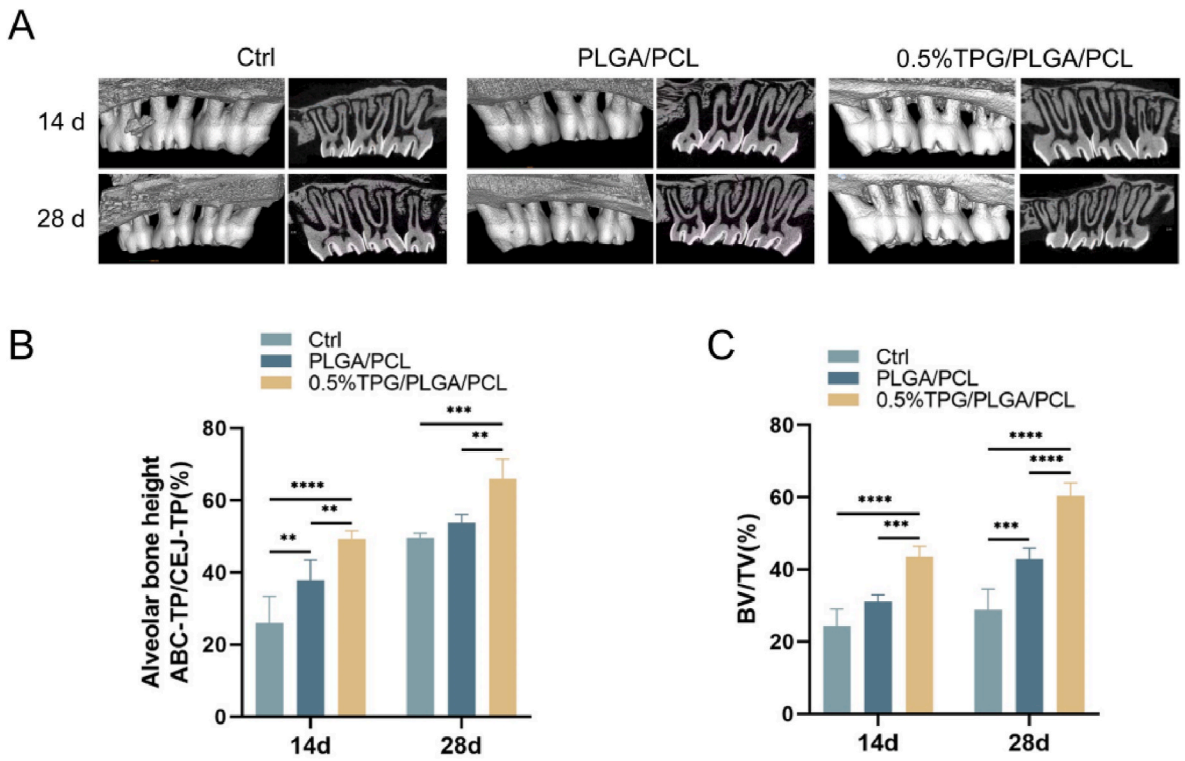

Fig. 8. Alveolar bone repair in a rat periodontitis model. (A) 2D and 3D reconstruction images of maxillary alveolar bone on 14 days and 28 days. (B) Relative fold change of CEJ-ABC. (C) Relative fold change of BV/TV. Variances were compared by one-way ANOVA. n ≥ 3. $^{*}P < 0.05$, $^{**}P < 0.01$, $^{***}P < 0.001$, $^{****}P < 0.001$.

anti-inflammatory M2 phenotype [37]. The mechanical properties of biological engineering materials are crucial for cell growth and tissue regeneration. The 0.5%TPG/PLGA/PCL fibrous membrane obtained heightened tensile strength and Young's modulus, attributed to the favorable mechanical properties of GO. In addition, the biomechanical properties of the extracellular matrix exert a significant impact on the modulation of cell phenotypes. Research indicates that mouse bone marrow-derived macrophages tend to polarize into the M1 phenotype when exposed to materials with small pore size and low hardness. In contrast, macrophages residing in materials with large pore size and high hardness demonstrate the M2 type characteristics [38]. Therefore, M2-type polarization induced by 0.5%TPG/PLGA/PCL may also be related to surface pore size and hardness.

Host immune response plays a critical role in the progression and destruction of periodontitis [39]. Macrophages, integral components of the innate immunity, are widely distributed throughout human tissues and serve as the frontline defense against pathogen microorganism invasion and infection [40]. The RAW 264.7 cell line, serving as a model macrophage cell line has found widespread utility in biomedicine and biomaterials research [41–43]. The results of CLSM and SEM indicated that nTPG/PLGA/PCL fibrous membranes could provide compatible adhesion surfaces for the growth of RAW 264.7 and hPDLSCs (Figs. 2A and 5D). PLGA and PCL are popular biocompatible polymers [44–46], and TPG reduced by TPs has better biocompatibility than GO [23,47]. The high activity in both RAW 264.7 and hPDLSCs in CCK-8 test demonstrated that nTPG/PLGA/PCL fibrous membranes can meet the cell compatibility criteria of biomaterials [34]. Furthermore, SEM images revealed that macrophages adhered closely to nTPG/PLGA/PCL fibrous membranes with extending pseudopods. The healing-promoting M2 phenotype, has been reported to be associated with increased cell elongation [48,49]. Interestingly, the cells on the nTPG/PLGA/PCL excluding 0.8%TPG/PLGA/PCL, displayed a relatively elongated shape. These results suggested that PLGA/PCL fibrous membranes, with or without TPG, exhibited cytocompatibility and were conducive to cell attachment and growth.

Macrophages exhibited remarkable plasticity and pluripotency, adopting different subtypes in distinct microenvironments and fulfilling unique functions [50,51], therefore, also affected the occurrence and development of various diseases and bone metabolism. Macrophages can be broadly categorized into two types: classical activation (M1) and alternative activation (M2). M1, often referred to as "pro-inflammatory" macrophages, possess robust antigen-presenting, bactericidal and pro-inflammatory effects, but also often cause damage to neighboring tissues [52–54]. M2, known as "anti-inflammatory" macrophages, play pivotal roles in angiogenesis, anti-inflammatory responses, and the promotion of tissue repair and wound healing [52,54–56]. There is increasing research evidence supporting that graphene-based materials affect the immune system to regulate the outcomes of tissue repair and regeneration [57,58]. Immune cells can be induced to release inflammatory mediators or growth factors, and engaging in different stages of tissue repair process [59,60]. We observed that the combination of LPS and IFN-γcould induce RAW 264.7 cells to polarize into the M1 phenotype, which led to an increase in the secretion of inflammatory factors. The 0.5%TPG/PLGA/PCL inhibited the polarization of the M1 phenotype while concurrently facilitating the transition to the M2 phenotype (Fig. 3B). Macrophages can produce BMP-2 to regulate bone formation [58]. We detected the expression of BMP-2 regulated by fibrous membranes by qRT-PCR. As shown in Fig. 3B, under the inflammatory stimulation, the BMP-2 mRNA levels of RAW 264.7 cells treated with the fibrous membranes were significantly increased compared to control group. Overall, 0.5%TPG/PLGA/PCL performed better in regulating the expression of inflammatory cytokines and BMP-2 compared to others.

Macrophage polarization is a intricate process influenced by multifactorial interactions, governed by a variety of signaling molecules and their corresponding pathways [29–31,61]. In this investigation, our findings suggested that LPS and IFN-γinduced the activation of PI3K/AKT and NF-κB signal pathways in vitro, and 0.5%TPG/PLGA/PCL effectively inhibited this activation (Fig. 4A and B). Further experimentation revealed that both the PI3K/Akt activator 740Y-P and the

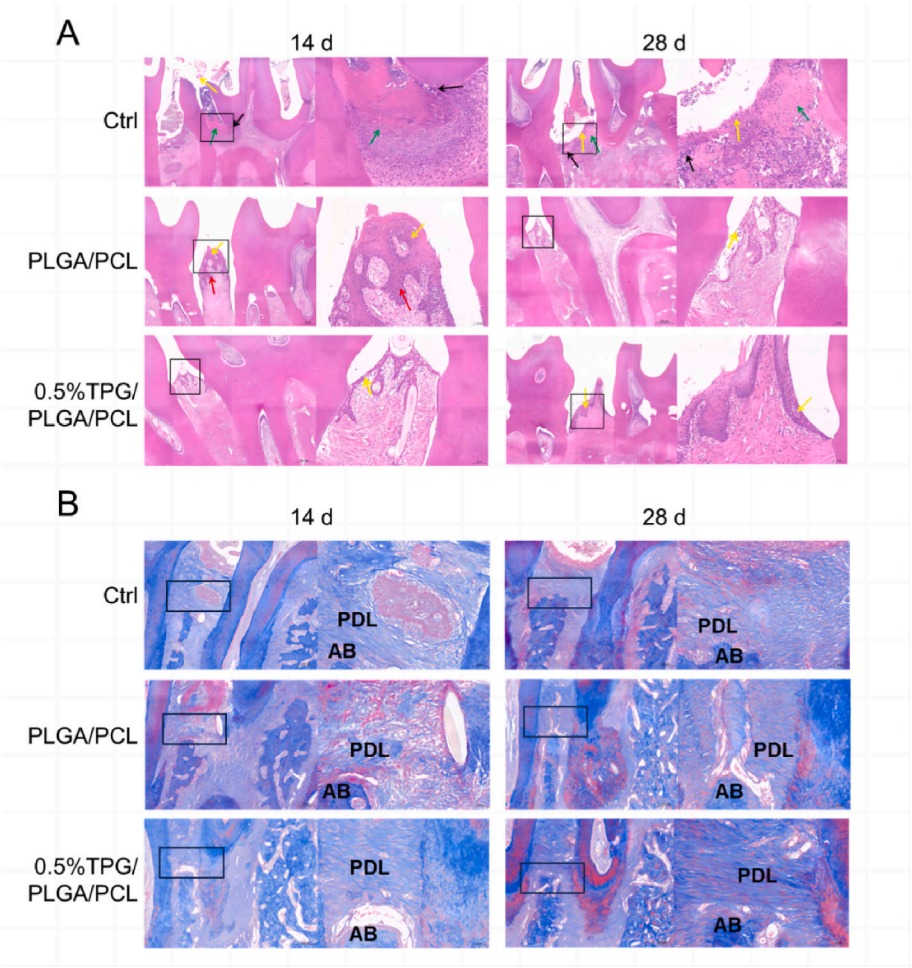

Fig. 9. Histology illustration images of the rat maxillary. (A) H&E staining of maxilla tissue section. (Scale bar = 50 μm. The black framed area was the enlarged area which was exhibited on the right. Scale bar = 200 μm. The yellow arrow pointed and red arrow pointed gingival epithelium and epithelial ridges while the green arrow showed and the black arrow showed the area of necrosis and inflammatory cells separately). (B) Masson trichrome staining of maxilla tissue section. (Scale bar = 50 μm. AB represents alveolar bone and PDL represents periodontal ligament. The black framed area was the enlarged area which was exhibited on the right. Scale bar = 200 μm). (For interpretation of the references to colour in this figure legend, the reader is referred to the Web version of this article.)

NF-κB activator PMA partially attenuated the signaling molecules of 0.5%TPG/PLGA/PCL (Fig. 4C). These results suggested that the 0.5% TPG/PLGA/PCL inhibited M1 macrophages polarization and expression of inflammatory factors via the suppression of the PI3K/Akt and NF-κB signaling pathways. Presently, numerous studies have focused on the development of drugs or biomaterials to regulate the function of macrophages [9,62–64]. It is imperative to delve into more potential mechanisms of macrophages in anti-inflammation, bone destruction and bone repair in periodontitis.

Considering the potential regulatory impact of 0.5%TPG/PLGA/PCL on macrophages, we speculated that it might influence the differentiation of hPDLSCs by modulating the periodontal immune microenvironment. Therefore, two distinct culture systems were constructed in our study, and the osteo/cementogenic and osteoclastic differentiation of hPDLSCs in different media were analyzed (Figs. 6 and 7). Results revealed that under both experimental conditions, 0.5%TPG/PLGA/PCL effectively promoted the cementoblastic differentiation of the hPDLSCs. This suggests that the cementoblastic effect of 0.5%TPG/PLGA/PCL on hPDLSCs was relatively less affected by the immune microenvironment of macrophages. However, the osteogenic effects were enhanced only under the influence of macrophages. These findings implied that 0.5% TPG/PLGA/PCL may play a critical role in promoting cementoblastic differentiation, independent of the immune microenvironment. However, its capacity to enhance osteogenic differentiation appears to be contingent on the presence and influence of macrophages. Studies have proved that GO can promote bone tissue regeneration by regulating the polarization of macrophages, stimulating the OSM signaling pathway and promote angiogenesis by VEGF signaling pathway [29]. Additional studies have shown that the conditioned medium from GO-RAW264.7 enhances osteogenic differentiation of BMSCs [65]. This underscores the intricate interplay between biomaterials, immune responses, and stem cell differentiation in the context of restoration of periodontal structures.

Currently, in the field of periodontal tissue regeneration research, the most common approach involves creating acute periodontal defect models through direct bone removal or the construction of cranial models [66]. However, acute periodontal defect models cannot adequately simulate the complexity of chronic periodontitis, as they do not accurately replicate the intricate interactions affecting the alveolar bone, periodontal ligment, and cementum [67]. Ligation, on the other hand, effectively induces alveolar bone resorption and periodontal inflammatory responses. This approach provided a more representative and clinically relevant model for research.

In our study (Fig. 9), the implantation of the 0.5%TPG/PLGA/PCL fibrous membrane into a rat periodontital defect model resulted in substantial bone formation. This newly formed bone effectively covered the root bifurcation and restored the height of the alveolar crest. In IHC and IF positive staining experiment, the osteogenesis-related markers

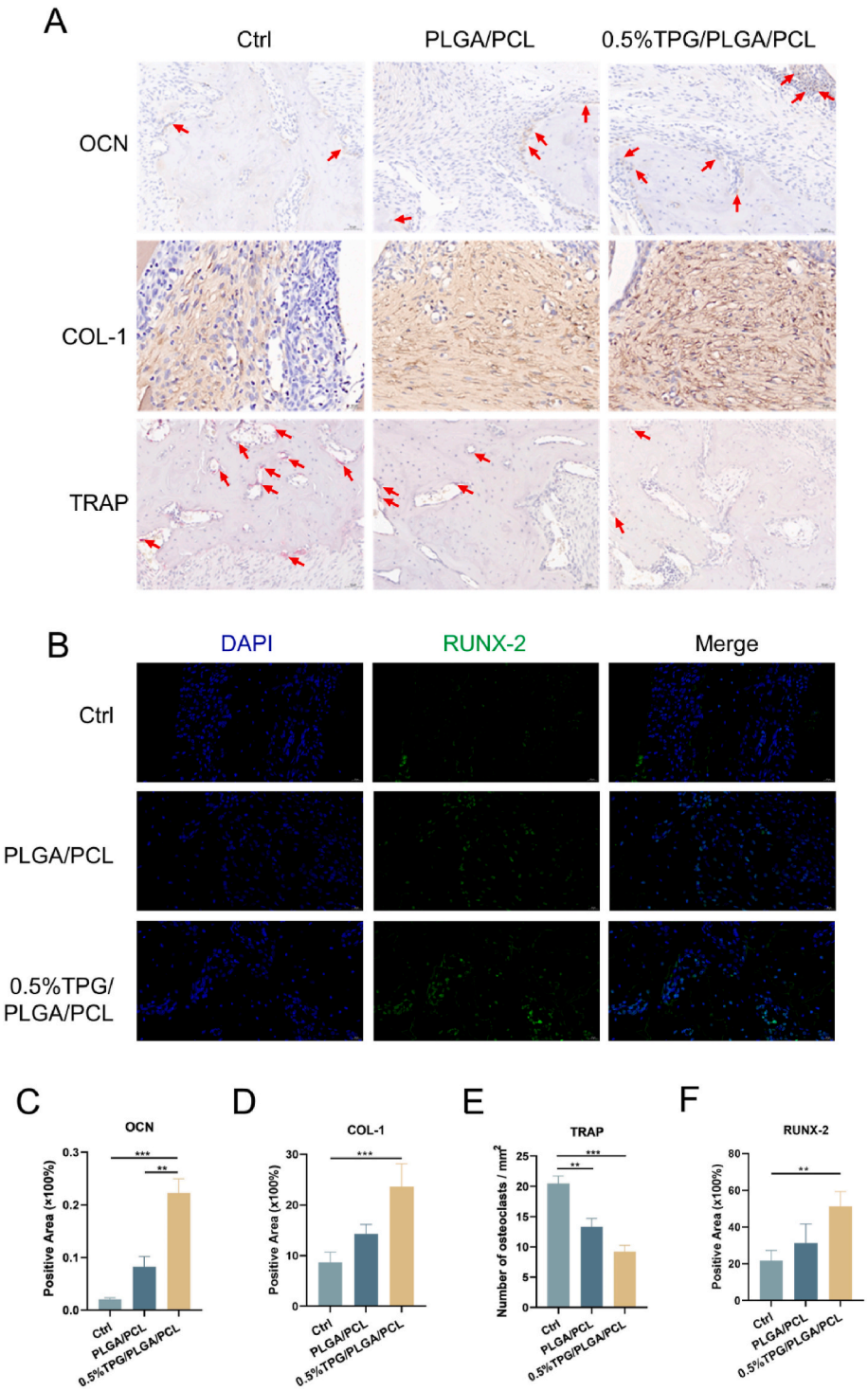

Fig. 10. Immunohistochemistry and immunofluorescence images and statistical analysis of the periodontal defect of the rat mandibular sections. (A) Immunohistochemistry staining of OCN, TRAP staining of osteoclasts and COL-1. (The arrows indicated OCN positive cells and TRAP-positive multinucleated osteoclasts. Scale bar = 50 μm for OCN and TRAP, Scale bar = 20 μm for COL-1) (B) Immunofuorescence staining images of RUNX-2. (Scale bar = 20 μm) (C) The positive area of OCN for 28 day. (D)The positive area of COL-1for 28 day. (E) The relative number of TRAP-positive cells in 1*1mm2 for 28 day. (F)The positive area of RUNX-2 for 28 day. Variances were compared by one-way ANOVA. n ≥ 3. $^{**}P < 0.01$, $^{***}P < 0.001$.

OCN, and RUNX-2 were highly expressed in the 0.5%TPG/PLGA/PCL group. The role of OCN, RUNX-2 with respect to bone formation, repair and regeneration has been well established [68]. Therefore, their upregulation in the presence of 0.5%TPG/PLGA/PCL membranes indicated continued osteoinductive stimulation of the host system resulting in better regeneration of tissue.

To ensure the functional stability and biomechanical loading of periodontium, periodontal tissue regeneration needs the functional restoration of the structure of cementum-periodontal ligament-alveolar bone complex [69]. COL-1 staining was perfomed to evaluate the regeneration of periodontal ligament, compared with the control group, the 0.5%TPG/PLGA/PCL group showed an increase expression of COL-1. The cementum marker BMP-2 was also tested in each group. Based on the current immunohistochemical images observed, the

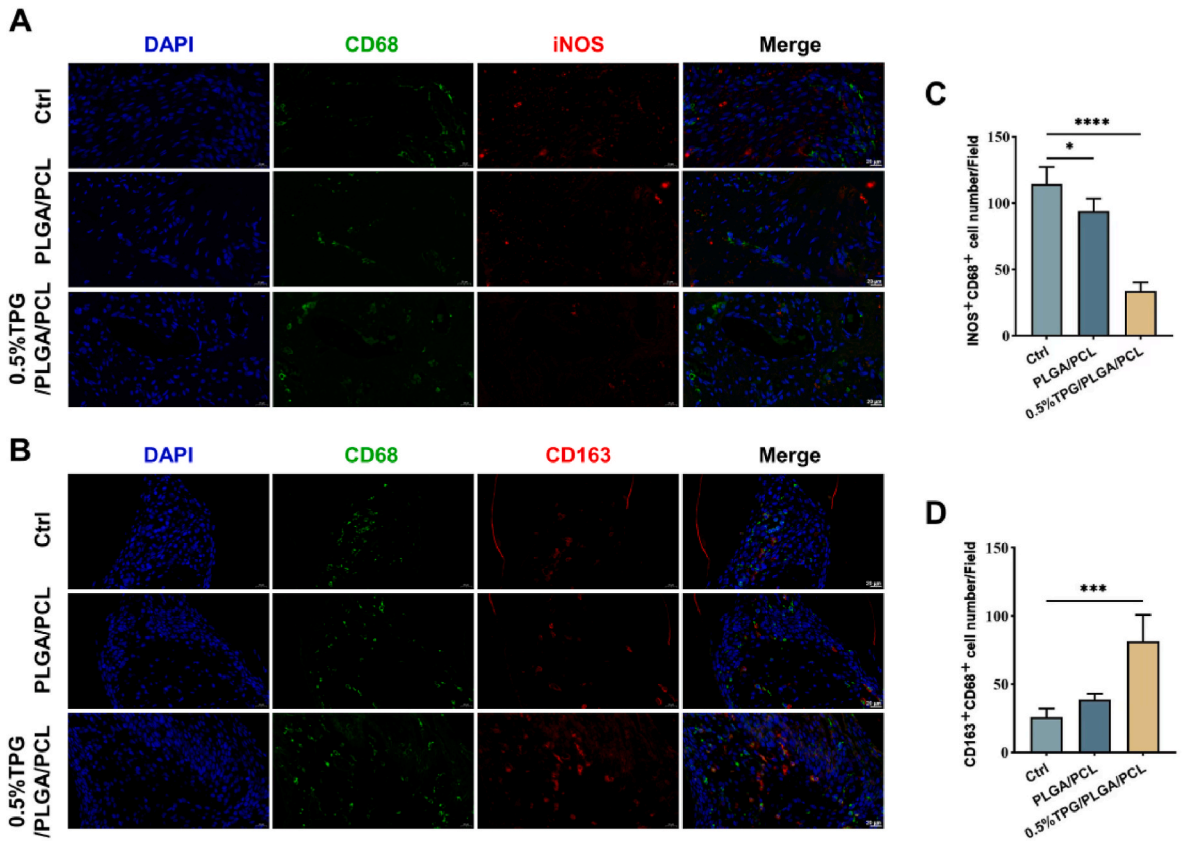

Fig. 11. Double-labeled immunofluorescence staining images of macrophage phenotype in the defect areas. (A) Immunofluorescence staining for iNOS and CD68. (The iNOS was marked by red fluorescence, and the CD68 was marked by green fluorescence. Cell nuclei were stained by DAPI with blue fluorescence. Scale bar = 20 μm) (B) Immunofluorescence staining for CD163 and CD68. (The CD163 was marked by red fluorescence, and the CD68 was marked by green fluorescence. Cell nuclei were stained by DAPI with blue fluorescence. Scale bar = 20 μm) (C,D) Statistical summary of the population of $iNOS^{+}CD68^{+}$ and $CD163^{+}CD68^{+}$. Variances were compared by one-way ANOVA. n ≥ 3. $^{*}P < 0.05$, $^{**}P < 0.01$, $^{***}P < 0.001$, $^{****}P < 0.001$. (For interpretation of the references to colour in this figure legend, the reader is referred to the Web version of this article.)

positive areas of 0.5%TPG/PLGA/PCL group were the most obvious (Supplementary Figure 4).

The modulation of macrophage functional phenotypes, specifically the transition between M1 and M2 phenotypes, is essential for maintaining macrophage function and homeostasis in tissue environments [70,71]. We explored the potential effect of 0.5%TPG/PLGA/PCL on macrophage polarization in vivo and found out it can inhibit M1 polarization and promote M2 polarization. The consistency between the results of in vitro and in vivo experiments demonstrated that 0.5% TPG/PLGA/PCL can reduce the damage caused by inflammation and promote periodontol tissue regeneration [62].

In summary, our study demonstrates that the 0.5%TPG/PLGA/PCL membrane has the capacity to modulate the polarization phenotype of macrophages. This regulatory influence, in turn, modulates the osteoblastic and cementoblastic differentiation of periodontal stem cells, ultimately guiding the regeneration of periodontal tissue. In order to achieve future clinical translation, more effort is needed to evaluate and upgarde the porosity, hydrophilicity, degradation and swelling rate of the 0.5%TPG/PLGA/PCL membranes. Such exploration aims to synergistically enhance the regenerative potential of periodontal tissue.

5. Conclusions

In summary, we constructed nTPG/PLGA/PCL fibrous membranes to modulate the immune microenvironment in periodontitis, aiming to optimize periodontal regeneration. The incorporation of TPG enhanced the physical and mechanical properties of the fibrous membrane. These membranes demonstrated excellent cytocompatibility, promoting cell adhesion and growth. Notably, under inflammatory conditions, the 0.5%TPG/PLGA/PCL fibrous membrane exhibited potent effects on the osteogenesis of hPDLSCs compared to the PLGA/PCL membrane. Additionally, our findings suggest that the immunomodulatory effects of 0.5%TPG/PLGA/PCL may be attributed to the suppression of the PI3K/AKT and NF-κB signaling pathways to suppress RAW 264.7 M1 polarization. This study is anticipated to establish a theoretical foundation for the future clinical application of TPG based polymer fibrous membranes.

Statement of significance

This project prepared a novel nTPG/PLGA/PCL nanofiber membrane and elucidated its mechanism of further regulating the functional differentiation of periodontal stem cells by regulating the polarization of macrophages. Barrier membrane not only has great physical barrier effect, but also has high immunomodulatory and bone-inducing properties. Therefore, we believe that this study will stimulate more scientific research to effectively promote periodontal regeneration.

CRediT authorship contribution statement

Xiang Han: Writing – original draft, Methodology, Investigation, Formal analysis, Data curation. **Feiyang Wang:** Writing – original draft, Investigation, Formal analysis, Data curation. **Yuzhuo Ma:** Resources, Methodology, Investigation. **Xuerong Lv:** Methodology, Investigation. **Kewei Zhang:** Resources, Methodology. **Yue Wang:** Resources, Formal analysis. **Ke Yan:** Resources, Methodology. **Youmin Mei:** Validation, Supervision. **Xiaoqian Wang:** Writing – review & editing, Supervision,

Conceptualization.

Declaration of competing interest

The authors declare that they have no known competing financial interests or personal relationships that could have appeared to influence the work reported in this paper.

Data availability

No data was used for the research described in the article.

Acknowledgement

This work was supported by National Natural Science Foundation of China (82101018), Jiangsu Province Capability Improvement Project through Science, Technology and Education-Jiangsu Provincial Research Hospital Cultivation Unit (YJXYYJSDW4), Jiangsu Provincial Medical Innovation Center (CXZX202227), Jiangsu Province Key Laboratory of Oral Diseases, Nanjing Medical University (JSKLOD-KF-1908).

List of abbreviations

abbreviation	*full name*
ALP	alkaline phosphatase
Arg-1	arginase 1
BMP-2	bone morphogenetic protein-2
CAP	cementum attachment protein
CCK-8	cell counting kit 8
CEMP-1	cementum protein 1
CLSM	laser Scanning Confocal Microscopy
CM	conditioned medium
COL-1	type I collagen
CPC	cetylpyridinium chloride
DMEM	dulbecco's modified eagle medium
FBS	fetal bovine serum
GAPDH	glyceraldehyde-3-phosphate dehydrogenase
GO	graphene oxide
GTR	guided tissue regeneration
hPDLSCs	human periodontal ligament cells
IFN-γ	Interferon-γ
IL-6	Interleukin-6
IL-10	Interleukin-10
iNOS	inducible nitric oxide sythase
LPS	lipopolysaccharide
OCN	osteocalcin
OPG	osteoprotegerin
OM	osteogenicinduced medium
PBS	phosphate buffer solution
PCL	poly(ε-caprolactone)
PLGA	poly(lactic-co-glycolic acid)
PMSF	phenylmethylsulfonyl fluoride
PVDF	polyvinylidene fluoride
rGO	reduced Graphene Oxide
RANKL	receptor activator of nuclear factor-κ B ligand
ROS	reactive oxygen species
RUNX2	runt-related transcription factor 2
RNA	ribonucleic acid
SEM	scanning electron microscope
TNF-α	tumor necrosis factor alpha
TPG	tea polyphenols functional graphene oxide
α-MEM	α-minimum essential medium alpha

Appendix A. Supplementary data

Supplementary data to this article can be found online at https://doi.org/10.1016/j.mtbio.2024.101036.

References

[1] S.P. Zhang, N. Yu, R.M. Arce, Periodontal inflammation: integrating genes and dysbiosis, Periodontol. 2000 82 (1) (2020) 129–142.
[2] P.E. Petersen, H. Ogawa, The global burden of periodontal disease: towards integration with chronic disease prevention and control, Periodontol. 2000 60 (2012) 15–39.
[3] J.D. Beck, K.L. Moss, T. Morelli, S. Offenbacher, Periodontal profile class is associated with prevalent diabetes, coronary heart disease, stroke, and systemic markers of C-reactive protein and interleukin-6, J. Periodontol. 89 (2) (2018) 157–165.
[4] S. Jepsen, J.G. Caton, J.M. Albandar, N.F. Bissada, P. Bouchard, P. Cortellini, K. Demirel, M. de Sanctis, C. Ercoli, J.Y. Fan, N.C. Geurs, F.J. Hughes, L.J. Jin, A. Kantarci, E. Lalla, P.N. Madianos, D. Matthews, M.K. McGuire, M.P. Mills, P. M. Preshaw, M.A. Reynolds, A. Sculean, C. Susin, N.X. West, K. Yamazaki, Periodontal manifestations of systemic diseases and developmental and acquired conditions: consensus report of workgroup 3 of the 2017 world workshop on the classification of periodontal and peri-implant diseases and conditions, J. Clin. Periodontol. 45 (2018) S219–S229.
[5] F.R.M. Leite, G.G. Nascimento, F. Scheutz, R. López, Effect of smoking on periodontitis: a systematic review and meta-regression, Am. J. Prev. Med. 54 (6) (2018) 831–841.
[6] L. Wu, S.Q. Zhang, L. Zhao, Z.H. Ren, C.Y. Hu, Global, regional, and national burden of periodontitis from 1990 to 2019: results from the Global Burden of Disease study 2019, J. Periodontol. 93 (10) (2022) 1445–1454.
[7] F.Q. Bui, C.L.C. Almeida-da-Silva, B. Huynh, A. Trinh, J. Liu, J. Woodward, H. Asadi, D.M. Ojcius, Association between periodontal pathogens and systemic disease, Biomed. J. 42 (1) (2019) 27–35.
[8] X.T. He, X. Li, Y. Xia, Y. Yin, R.X. Wu, H.H. Sun, F.M. Chen, Building capacity for macrophage modulation and stem cell recruitment in high-stiffness hydrogels for complex periodontal regeneration: experimental studies *in vitro* and in rats, Acta Biomater. 88 (2019) 162–180.
[9] C. Ni, J. Zhou, N. Kong, T.Y. Bian, Y.H. Zhang, X.F. Huang, Y. Xiao, W.R. Yang, F. H. Yan, Gold nanoparticles modulate the crosstalk between macrophages and periodontal ligament cells for periodontitis treatment, Biomaterials 206 (2019) 115–132.
[10] T. Spinell, J. Saliter, B. Hackl, K. Unger, R. Hickel, M. Folwaczny, In-vitro cytocompatibility and growth factor content of GBR/GTR membranes, Dent. Mater. 35 (7) (2019) 963–969.
[11] C.C. Chen, S.Y. Lee, N.C. Teng, H.T. Hu, P.C. Huang, J.C. Yang, In vitro and in vivo studies of hydrophilic electrospun PLA95/-TCP membranes for guided tissue regeneration (GTR) applications, Nanomaterials 9 (4) (2019).
[12] S.S. Dehnavi, M. Mehdikhani, M. Rafienia, S. Bonakdar, Preparation and in vitro evaluation of polycaprolactone/PEG/bioactive glass nanopowders nanocomposite membranes for GTR/GBR applications, Mater. Sci. Eng., C 90 (2018) 236–247.
[13] Y. Gao, S. Wang, B.Y. Shi, Y.X. Wang, Y.M. Chen, X.Y. Wang, E.S. Lee, H.B. Jiang, Advances in modification methods based on biodegradable membranes in guided bone/tissue regeneration: a review, Polymers 14 (5) (2022).
[14] M. Ndumiso, N. Buchtová, L. Husselmann, G. Mohamed, A. Klein, M. Aucamp, D. Canevet, S. D'Souza, R.E. Maphasa, F. Boury, A. Dube, Comparative whole corona fingerprinting and protein adsorption thermodynamics of PLGA and PCL nanoparticles in human serum, Colloids Surf. B Biointerfaces 188 (2020).
[15] Z.T. Wang, R.M. Liang, X.F. Jiang, J.L. Xie, P.A. Cai, H.M. Chen, X.T. Zhan, D. Q. Lei, J.M. Zhao, L. Zheng, Electrospun PLGA/PCL/OCP nanofiber membranes promote osteogenic differentiation of mesenchymal stem cells (MSCs), Mater. Sci. Eng., C 104 (2019).
[16] A.E. Ashour, M. Badran, A. Kumar, T. Hussain, I.A. Alsarra, A.E.B. Yassin, Physical PEGylation enhances the cytotoxicity of 5-fluorouracil-loaded PLGA and PCL nanoparticles, Int. J. Nanomed. 14 (2019) 9259–9273.
[17] M. Toledano-Osorio, F.J. Manzano-Moreno, C. Ruiz, M. Toledano, R. Osorio, Testing active membranes for bone regeneration: a review, J. Dent. 105 (2021).
[18] S.S.R. Vuppaladadium, T. Agarwal, S. Kulanthaivel, B. Mohanty, C.S. Barik, T. K. Maiti, S. Pal, K. Pal, I. Banerjee, Silanization improves biocompatibility of graphene oxide, Mater. Sci. Eng., C 110 (2020).
[19] T.K. Chang, Y.C. Lu, S.T. Yeh, T.C. Lin, C.H. Huang, C.H. Huang, In vitro and in vivo biological responses to graphene and graphene oxide: a murine calvarial animal study, Int. J. Nanomed. 15 (2020) 647–659.
[20] X.L. Liu, B. Yan, Y. Li, X.W. Ma, W.B. Jiao, K.J. Shi, T.B. Zhang, S.Z. Chen, Y. He, X. J. Liang, H.M. Fan, Graphene oxide-grafted magnetic nanorings mediated magnetothermodynamic therapy favoring reactive oxygen species-rebated immune response for enhanced antitumor efficacy, ACS Nano 14 (2) (2020) 1936–1950.
[21] A. Sinha, Y. Choi, M.H. Nguyen, T.L. Nguyen, S.W. Choi, J. Kim, A 3D macroporous alginate graphene scaffold with an extremely slow release of a loaded cargo for in situ long-term activation of dendritic cells, Adv. Healthcare Mater. 8 (5) (2019).
[22] X.L. Yang, Y. Zhang, W.J. Lai, Z.C. Xiang, B. Tu, D. Li, X.H. Nan, C.Y. Chen, Z.Y. Hu, Q.J. Fang, Proteomic profiling of RAW264.7 macrophage cells exposed to graphene oxide: insights into acute cellular responses, Nanotoxicology 13 (1) (2019) 35–49.

[23] X.Q. Wang, L.Y. Hao, C.L. Zhang, J. Chen, P. Zhang, High efficient anti-cancer drug delivery systems using tea polyphenols reduced and functionalized graphene oxide, J. Biomater. Appl. 31 (8) (2017) 1108–1122.

[24] Z.Y. Ji, X.P. Shen, J.L. Yang, G.X. Zhu, K.M. Chen, A novel reduced graphene oxide/Ag/CeO_2 ternary nanocomposite: green synthesis and catalytic properties, Appl. Catal. B Environ. 144 (2014) 454–461.

[25] R. Serôdio, S.L. Schickert, A.R. Costa-Pinto, J.R. Dias, P.L. Granja, F. Yang, A. L. Oliveira, Ultrasound sonication prior to electrospinning tailors silk fibroin/PEO membranes for periodontal regeneration, Mater. Sci. Eng., C 98 (2019) 969–981.

[26] S.S. Ren, Y.F. Yao, H. Zhang, R.R. Fan, Y.J. Yu, J. Yang, R. Zhang, C. Liu, W.B. Sun, L.Y. Miao, Aligned fibers fabricated by near-field electrospinning influence the orientation and differentiation of hPDLSCs for periodontal regeneration, J. Biomed. Nanotechnol. 13 (12) (2017) 1725–1734.

[27] M. Ranjbar-Mohammadi, M. Zamani, M.P. Prabhakaran, S.H. Bahrami, S. Ramakrishna, Electrospinning of PLGA/gum tragacanth nanofibers containing tetracycline hydrochloride for periodontal regeneration, Mater. Sci. Eng., C 58 (2016) 521–531.

[28] S.U. Rahman, J.H. Oh, Y.D. Cho, S.H. Chung, G. Lee, J.H. Baek, H.M. Ryoo, K. M. Woo, Fibrous topography-potentiated canonical wnt signaling directs the odontoblastic differentiation of dental pulp-derived stem cells, ACS Appl. Mater. Interfaces 10 (21) (2018) 17526–17541.

[29] N. Jain, J. Moeller, V. Vogel, Mechanobiology of macrophages: how physical factors coregulate macrophage plasticity and phagocytosis, in: M.L. Yamush (Ed.), Annual Review of Biomedical Engineering, Vol vol. 212019, pp. 267-297.

[30] X. Li, X.T. He, D.Q. Kong, X.Y. Xu, R.X. Wu, L.J. Sun, B.M. Tian, F.M. Chen, M2 macrophages enhance the cementoblastic differentiation of periodontal ligament stem cells via the akt and JNK pathways, Stem Cell. 37 (12) (2019) 1567–1580.

[31] Z.Y. Wang, K. Maruyama, Y. Sakisaka, S. Suzuki, H. Tada, M. Suto, M. Saito, S. Yamada, E. Nemoto, Cyclic stretch force induces periodontal ligament cells to secrete exosomes that suppress IL-1β production through the inhibition of the NF-κB signaling pathway in macrophages, Front. Immunol. 10 (2019).

[32] N. Chen, L.L. Tian, L.M. He, S. Ramakrishna, Nanobiomaterials for neural regeneration, Neural Regeneration Research 11 (9) (2016) 1372–1374.

[33] X.W. Xu, S.S. Ren, L. Li, Y. Zhou, W.Z. Peng, Y. Xu, Biodegradable engineered fiber scaffolds fabricated by electrospinning for periodontal tissue regeneration, J. Biomater. Appl. 36 (1) (2021) 55–75.

[34] Y. Wang, W.G. Cui, J. Chou, S.Z. Wen, Y.L. Sun, H.Y. Zhang, Electrospun nanosilicates-based organic/inorganic nanofibers for potential bone tissue engineering, Colloids Surf. B Biointerfaces 172 (2018) 90–97.

[35] B.J. Ma, S. Zhang, F. Liu, J.Z. Duan, S.C. Wang, J. Han, Y.H. Sang, X.Q. Yu, D. Li, W. Tang, S.H. Ge, H. Liu, One-dimensional hydroxyapatite nanostructures with tunable length for efficient stem cell differentiation regulation, ACS Appl. Mater. Interfaces 9 (39) (2017) 33717–33727.

[36] W. Florjanski, S. Orzeszek, A. Olchowy, N. Grychowska, W. Wieckiewicz, A. Malysa, J. Smardz, M. Wieckiewicz, Modifications of polymeric membranes used in guided tissue and bone regeneration, Polymers 11 (5) (2019).

[37] X.Y. Li, B.J. Ma, J.H. Li, L.L. Shang, H. Liu, S.H. Ge, A method to visually observe the degradation-diffusion-reconstruction behavior of hydroxyapatite in the bone repair process, Acta Biomater. 101 (2020) 554–564.

[38] K.M. Hotchkiss, G.B. Reddy, S.L. Hyzy, Z. Schwartz, B.D. Boyan, R. Olivares-Navarrete, Titanium surface characteristics, including topography and wettability, alter macrophage activation, Acta Biomater. 31 (2016) 425–434.

[39] S.M. Jiang, C. Lyu, P. Zhao, W.J. Li, W.Y. Kong, C.Y. Huang, G.M. Genin, Y.N. Du, Cryoprotectant enables structural control of porous scaffolds for exploration of cellular mechano-responsiveness in 3D, Nat. Commun. 10 (2019).

[40] D.D. Bosshardt, A. Sculean, Does periodontal tissue regeneration really work? Periodontol. 2000 51 (2009) 208–219.

[41] 倪璨 葛叡扬, 闫福华 杨琨, 巨噬细胞极化在牙周炎发病及治疗中的作用 [J/OL] 中国组织工程研究 28 (20) (2024) 3246–3251.

[42] Z.T. Chen, C.T. Wu, W.Y. Gu, T. Klein, R. Crawford, Y. Xiao, Osteogenic differentiation of bone marrow MSCs by β-tricalcium phosphate stimulating macrophages via BMP2 signalling pathway, Biomaterials 35 (5) (2014) 1507–1518.

[43] Z.T. Chen, A. Bachhuka, S.W. Han, F. Wei, S. Lu, R.M. Visalakshan, K. Vasilev, Y. Xiao, Tuning chemistry and topography of nanoengineered surfaces to manipulate immune response for bone regeneration applications, ACS Nano 11 (5) (2017) 4494–4506.

[44] U.M. Graham, A.K. Dozier, D.J. Feola, M.T. Tseng, R.A. Yokel, Macrophage polarization status impacts nanoceria cellular distribution but not its biotransformation or ferritin effects, Nanomaterials 13 (16) (2023).

[45] H. Pauly, D. Kelly, K. Popat, J. Easley, R. Palmer, T.L.H. Donahue, Mechanical properties of a hierarchical electrospun scaffold for ovine anterior cruciate ligament replacement, J. Orthop. Res. 37 (2) (2019) 421–430.

[46] O. Gil-Castell, J.D. Badia, I. Ontoria-Oviedo, D. Castellano, P. Sepúlveda, A. Ribes-Greus, Polycaprolactone/gelatin-based scaffolds with tailored performance: *in vitro* and *in vivo* validation, Mater. Sci. Eng., C 107 (2020).

[47] P. He, Q. Zhong, Y. Ge, Z.Z. Guo, J.H. Tian, Y.H. Zhou, S. Ding, H. Li, C.R. Zhou, Dual drug loaded coaxial electrospun PLGA/PVP fiber for guided tissue regeneration under control of infection, Mater. Sci. Eng., C 90 (2018) 549–556.

[48] A. Ben Lagha, D. Grenier, Tea polyphenols protect gingival keratinocytes against TNF-α-induced tight junction barrier dysfunction and attenuate the inflammatory response of monocytes/macrophages, Cytokine 115 (2019) 64–75.

[49] L.D. Huyer, S. Pascual-Gil, Y.F. Wang, S. Mandla, B. Yee, M. Radisic, Advanced strategies for modulation of the material-macrophage interface, Adv. Funct. Mater. 30 (44) (2020).

[50] F.Y. McWhorter, T.T. Wang, P. Nguyen, T. Chung, W.F. Liu, Modulation of macrophage phenotype by cell shape, Proc. Natl. Acad. Sci. U.S.A. 110 (43) (2013) 17253–17258.

[51] M.N. Michalski, L.K. McCauley, Macrophages and skeletal health, Pharmacol. Ther. 174 (2017) 43–54.

[52] B.P. Sinder, A.R. Pettit, L.K. McCauley, Macrophages: their emerging roles in bone, J. Bone Miner. Res. 30 (12) (2015) 2140–2149.

[53] A. Mantovani, A. Sica, S. Sozzani, P. Allavena, A. Vecchi, M. Locati, The chemokine system in diverse forms of macrophage activation and polarization, Trends Immunol. 25 (12) (2004) 677–686.

[54] P.J. Murray, J.E. Allen, S.K. Biswas, E.A. Fisher, D.W. Gilroy, S. Goerdt, S. Gordon, J.A. Hamilton, L.B. Ivashkiv, T. Lawrence, M. Locati, A. Mantovani, F.O. Martinez, J.L. Mege, D.M. Mosser, G. Natoli, J.P. Saeij, J.L. Schultze, K.A. Shirey, A. Sica, J. Suttles, I. Udalova, J.A. van Ginderachter, S.N. Vogel, T.A. Wynn, Macrophage activation and polarization: nomenclature and experimental guidelines, Immunity 41 (1) (2014) 14–20.

[55] L.B. Ivashkiv, Epigenetic regulation of macrophage polarization and function, Trends Immunol. 34 (5) (2013) 216–223.

[56] S. Gordon, F.O. Martinez, Alternative activation of macrophages: mechanism and functions, Immunity 32 (5) (2010) 593–604.

[57] A. Varin, S. Gordon, Alternative activation of macrophages: immune function and cellular biology, Immunobiology 214 (7) (2009) 630–641.

[58] M. Orecchioni, C. Ménard-Moyon, L.G. Delogu, A. Bianco, Graphene and the immune system: challenges and potentiality, Adv. Drug Deliv. Rev. 105 (2016) 163–175.

[59] S.P. Mukherjee, M. Bottini, B. Fadeel, Graphene and the immune system: a romance of many dimensions, Front. Immunol. 8 (2017).

[60] T.A. Wynn, K.M. Vannella, Macrophages in tissue repair, regeneration, and fibrosis, Immunity 44 (3) (2016) 450–462.

[61] J.P. Cooke, Inflammation and its role in regeneration and repair A caution for novel anti-inflammatory therapies, Circ. Res. 124 (8) (2019) 1166–1168.

[62] X. Huang, T. Yu, C.J. Ma, Y.X. Wang, B.Y. Xie, D.Y. Xuan, J.C. Zhang, Macrophages play a key role in the obesity-induced periodontal innate immune dysfunction via nucleotide-binding oligomerization domain-like receptor protein 3 pathway, J. Periodontol. 87 (10) (2016) 1195–1205.

[63] X.T. He, X. Li, M. Zhang, B.M. Tian, L.J. Sun, C.S. Bi, D.K. Deng, H. Zhou, H.L. Qu, C.T. Wu, F.M. Chen, Role of molybdenum in material immunomodulation and periodontal wound healing: targeting immunometabolism and mitochondrial function for macrophage modulation, Biomaterials 283 (2022).

[64] Z. Zhuang, S. Yoshizawa-Smith, A. Glowacki, K. Maltos, C. Pacheco, M. Shehabeldin, M. Mulkeen, N. Myers, R. Chong, K. Verdelis, G.P. Garlet, S. Little, C. Sfeir, Induction of M2 macrophages prevents bone loss in murine periodontitis models, J. Dent. Res. 98 (2) (2019) 200–208.

[65] J. Zhou, S. Sun, Y. He, T.T. Yan, J.F. Sun, J. Pan, S.Y. Zhu, L.Q. Chen, P.F. Zhu, B. A. Xu, Y. Liu, Role of magnesium-doped calcium sulfate and β-tricalcium phosphate composite ceramics in macrophage polarization and osteo-induction, Odontology 110 (4) (2022) 735–746.

[66] D.T. Xue, E.M. Chen, H.M. Zhong, W. Zhang, S.D. Wang, M.U. Joomun, T.Y. Yao, Y. B. Tan, S.S. Lin, Q. Zheng, Z.J. Pan, Immunomodulatory properties of graphene oxide for osteogenesis and angiogenesis, Int. J. Nanomed. 13 (2018) 5799–5810.

[67] E.A. Trofin, P. Monsarrat, P. Kémoun, Cell therapy of periodontium: from animal to human? Front. Physiol. 4 (2013).

[68] A. Almubarak, K.K.K. Tanagala, P.N. Papapanou, E. Lalla, F. Momen-Heravi, Disruption of monocyte and macrophage homeostasis in periodontitis, Front. Immunol. 11 (2020).

[69] G.S. Baht, G.K. Hunter, H.A. Goldberg, Bone sialoprotein-collagen interaction promotes hydroxyapatite nucleation, Matrix Biol. 27 (7) (2008) 600–608.

[70] J.P. Barrett, D.A. Costello, J. O'Sullivan, T.R. Cowley, M.A. Lynch, Bone marrow-derived macrophages from aged rats are more responsive to inflammatory stimuli, J. Neuroinflammation 12 (2015).

[71] A. Almubarak, K.K.K. Tanagala, P.N. Papapanou, E. Lalla, F. Momen-Heravi, Disruption of monocyte and macrophage homeostasis in periodontitis, Front. Immunol. 11 (2020).